M.TECH (POWER ELECTRONICS & SYSTEMS) SATYAMIT KUMAR 2023

DESIGN AND MODELLING OF BOOST PFC AND SEPIC PFC FED HALF BRIDGE LLC RESONANT CONVERTER FOR ON BOARD CHARGING APPLICATION

DISSERTATION

SUBMITTED IN PARTIAL FULFILLMENT OF THE REQUIREMENTS

FOR THE AWARD OF THE DEGREE

OF

MASTER OF TECHNOLOGY

IN

POWER ELECTRONICS AND SYSTEMS

Submitted by

SATYAMIT KUMAR

2K21/PES/14

Under the supervision of

PROF. NARENDRA KUMAR II

ELECTRICAL ENGINEERING DEPARTMENT

DELHI TECHNOLOGICAL UNIVERSITY

(Formerly Delhi College of Engineering)

Bawana Road, Delhi-110042

MAY - 2023

DELHI TECHNOLOGICAL UNIVERSITY

(Formerly Delhi College of Engineering)

Bawana Road, Delhi-110042

CANDIDATE'S DECLARATION

I SATYAMIT KUAR, Roll No. 2K21/PES/14, Student of M. Tech Power electronics and systems, hereby declare that the Dissertation titled **"DESIGN AND MODELLING OF BOOST PFC AND SEPIC PFC FED HALF BRIDGE LLC RESONANT CONVERTER FOR ON BOARD CHARGING APPLICATION"** which is submitted by me to the Department of Electrical Engineering, Delhi Technological University, Delhi in partial fulfilment of the requirement for the award of the degree of Master of Technology, is original and not copied from any source without proper citation. This work has not previously formed the basis for the award of any Degree, Diploma Associateship, Fellowship or other similar title or recognition.

Place: Delhi **SATYAMIT KUMAR**

Date: 31 May, 2023 **2K21/PES/14**

DELHI TECHNOLOGICAL UNIVERSITY

(Formerly Delhi College of Engineering)

Bawana Road, Delhi-110042

CERTIFICATE

I hereby certify that the thesis titled **"DESIGN AND MODELLING OF BOOST PFC AND SEPIC PFC FED HALF BRIDGE LLC RESONANT CONVERTER FOR ON BOARD CHARGING APPLICATION"** Which is submitted by SATYAMIT KUMAR 2K21/PES/14 ELECTRICAL ENGINEERING DEPARTMENT, Delhi Technological University, Delhi, in partial fulfilment of the requirement for the award of the degree of Master of Technology, is a record of the Dissertation work carried out by the students under my supervision. To the best of my knowledge, this work has not been submitted in part or full for any Degree to this University or elsewhere.

Place: Delhi **PROF. NARENDRA KUMAR II**

Date: 31 May, 2023 (Supervisor)

DELHI TECHNOLOGICAL UNIVERSITY

(Formerly Delhi College of Engineering)

Bawana Road, Delhi-110042

ACKNOWLEDGEMENT

I would like to express my gratitude towards all the people who have contributed their precious time and effort to help me without whom it would not have been possible for me to understand and complete the Dissertation. I would like to thank **Prof. NARENDRA KUMAR II**, Department of Electrical Engineering, my Project guide, support, motivation and encouragement throughout the period this work was carried out. His readiness for consultation at all times, his educative comments, his concern and assistance even with practical things have been invaluable.

Place: Delhi **SATYAMIT KUMAR**

Date: 31 May, 2023 **2K21/PES/14**

ABSTRACT

This project describes a half-bridge LLC resonant converter followed by a power factor corrected (PFC) boost converter in an electric car battery. The suggested charger employs a boost converter as the front-end dc-dc converter, which operates in continuous conduction mode (CCM) of the input inductor to provide harmonic-free AC mains current. As the second stage, a Half-Bridge LLC resonant converter is used to accelerate battery charging. An active power factor controller (APFC) manages the DC-link voltage while also maintaining sinusoidal input current. Pulse frequency modulation (PFM) is used after the PI-controller to adjust the battery's output. On the MATLAB/Simulink platform, the proposed charger's steady-state and dynamic performance are evaluated for a range of supply voltage and load conditions.

In the above configuration with first stage as the PFC Boost converter the problem of high inrush current is there. Therefore, in the second part of this project, a PFC-SEPIC fed LLC resonant converter for an on-board private charging unit is proposed which eliminates this problem of high inrush current. The PFC-SEPIC converter at the input stage is intended to function in continuous conduction mode (CCM) and enhances power quality execution on alternating current mains for a vast span of output voltages and also provides capacitive isolation. The design for V_S = 85V and TDD less than 3.895% for varied input voltages and battery voltages at different loads, is affirmed using MATLAB/SIMULINK.

CONTENTS

LIST OF FIGURES

LIST OF TABLES

LIST OF SYSMBOL, ABBREBIATIONS

Symbols

Ω	ohm
%	Percentage
V	Volt
A	Ampere
mA	Milli ampere
n	Turns ratio
m	Ratio of inductance
Fn	Normalized Frequency
Rac	Equivalent Resistance
Lr	Resonant inductance
Cr	Resonant capacitance
T	Turns ratio
f_{sw}	Switching Frequency
f_r	Resonant frequency
Ro	Load resistance
Co	Output Capacitance
Vin1	Input Voltage
D	Duty ratio
mH	Milli Henry
uF	Micro Farad
Lm	Magnetizing inductance
P_o	Output Power
V_s	RMS value of Source Voltage

Abbreviations

CC	Constant Current
CV	Constant Voltage
CCCV	Constant current constant voltage
SEPIC	Single-Ended Primary Inductance Converter
LLC	Tank of inductances and capacitance
DC	Direct current
BMS	Battery management system
APFC	Active Power Factor Controller
PWM	Pulse Width Modulation
MOSFET	Metal oxide semiconductor field effect transistor
PFC	Power Factor Corrected
DCM	Discontinuous Conduction Mode
CCM	Continuous Conduction Mode
ZCS	Zero Current Switching
ZVS	Zero voltage switching
AC	Alternating current

CHAPTER 1
INTRODUCTION

1.1 Background

The cost of gasoline has continued to rise since the early 1990s. Based on research conducted by EIA (Energy Information Administration) between 1990 and 2014, as depicted in Figure 1.1, the price of gasoline has increased 3 times since 1991. This increase in gas prices contributes to higher expenses associated with traditional transportation methods.

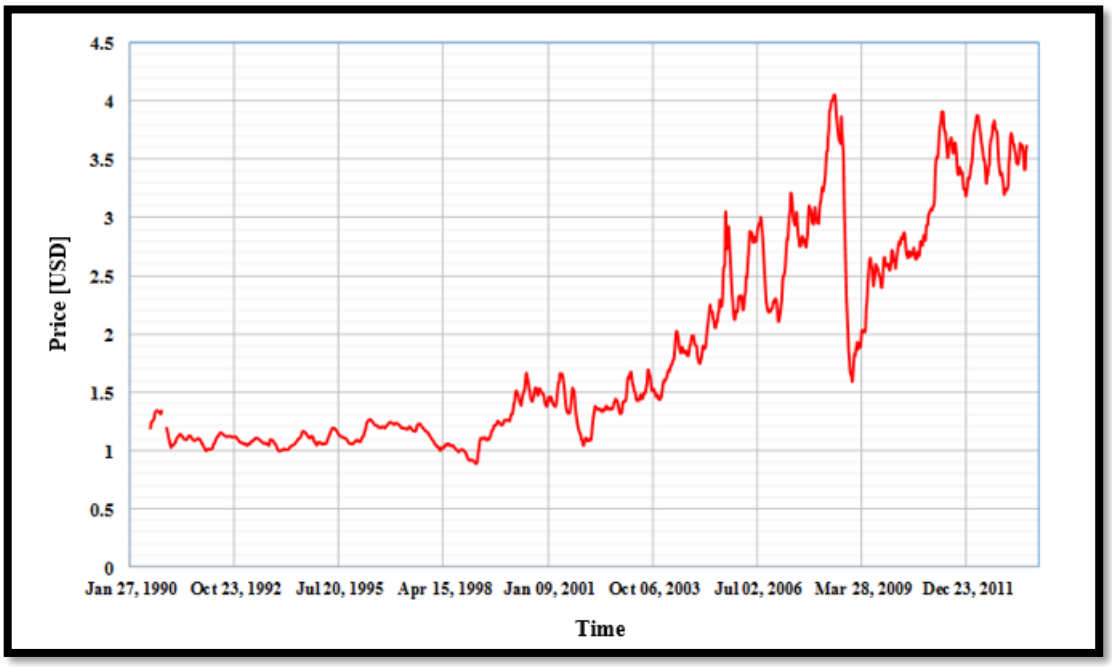

Fig. 1.1: The weekly retail prices of regular conventional gasoline in US

However, as material science & manufacturing battery technology continue to advance, the cost of batteries is progressively reducing, while their energy density is consistently increasing each year. This can be observed in Figure 1.2 [1]. Trends like these are driving the shift in transportation from traditional ICE vehicles to next generation of electrified drivetrain system. As a result, there is a growing focus on the development of advanced plugged-in hybrid electric vehicles (PHEVs) & electric vehicles(EVs) technologies.

Fig. 1.2: Energy density and Li-ion pricing

The official goal for the US is to have 1 billion EVs on road by 2025. [2]. Various policies for public have been enacted by governments for incentivizing the adoption of electric vehicles and promote the electrification of transportation systems [3]. Figure 1.3 presents a graphical representation of projected annual sales of light-duty electric vehicles globally. According to the chart, its anticipated that the sales of EVs will be increased by a factor of 46 by 2017 compared to the sales in 2011.

As the cost of batteries decreases, the price difference between conventional ICE vehicles & EVs will diminish, making EVs more financially accessible. However, ordinary consumers are increasingly concerned about the charging speed and the time it takes to recharge EV batteries. Unlike conventional ICE vehicles, which can be refueled in 3 to 5 minutes, recharging the battery pack of an EV takes significantly longer. Additionally, the limited availability of charging infrastructure acts as a barrier in the widescale adoption of EVs [4].

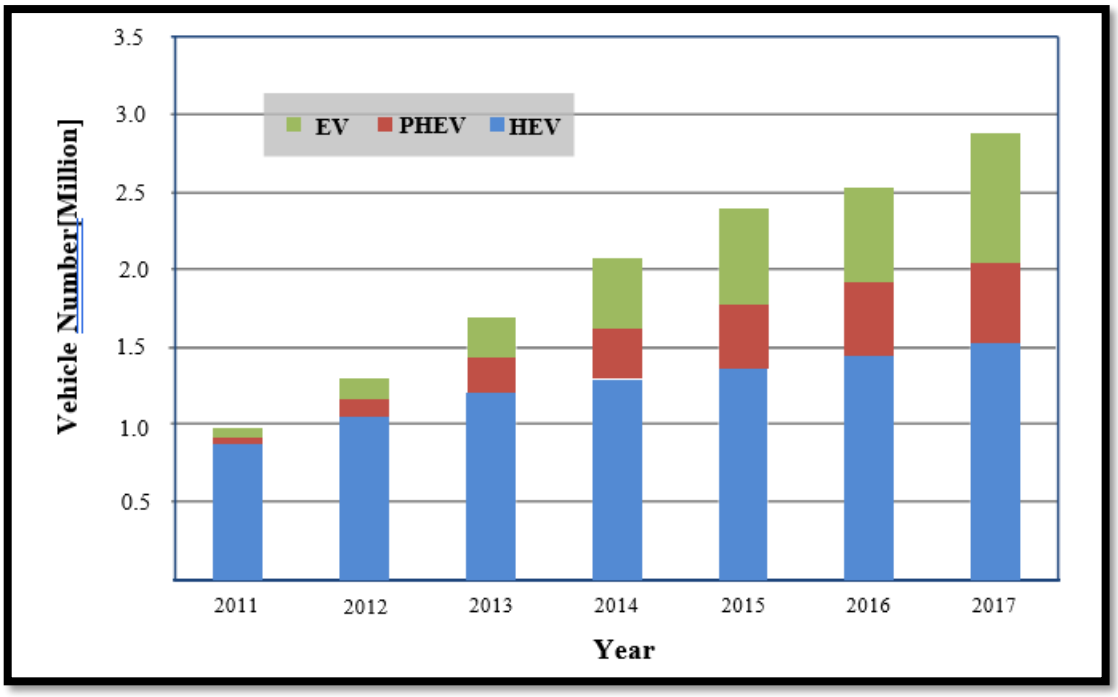

Fig. 1.3: Worldwide annual sale of light-duty EVs [5].

It is widely acknowledged that electric vehicles (EVs) offer several advantages over gas-engine vehicles, including regenerative braking capacity of motor, greater efficiency of energy conversion, reduced exhaust emissions, & lower levels of vibration and acoustic noise. The battery plays the important role in advancement & progress of PHEVs & EVs.

Fig.1.4: EV & its main components

An electric vehicle (EV), depicted in Figure 1.4 [6], is the kind of vehicle that is driven on electricity rather than relying on conventional fossil fuels like most vehicles on the road today. This electricity can be obtained from an external source and stored in a battery or produced onboard using fuel cells (FCs). The development of EVs dates back to 1834 when Thomas Davenport built the first battery-powered EV, a tricycle [7]. Remarkably, this development predates the foundation of ICE vehicles that utilize diesel or gasoline fuel. However, early EVs were deemed impractical and inefficient due to their considerable weight and lengthy charging times. Additionally, they became more expensive than ICE vehicles starting from around 1910, which resulted in the dominance of gasoline-based vehicles. But, concerns regarding the fossil fuels depletion & the negative environmental impact of greenhouse gases have brought renewed attention to the development of alternative-fuel vehicles. The urgency of developing such vehicles is evident not only to scientists but also to governments worldwide, as demonstrated by the ratification of the Kyoto Protocol by 183 countries (as of January 2009). Battery electric vehicles (BEVs) have emerged as an area of significant research interest for both scientific researchers & car manufacturers. The system architecture of hybrid electric vehicles (HEVs) and EVs is illustrated in Figure 1.5 [6].

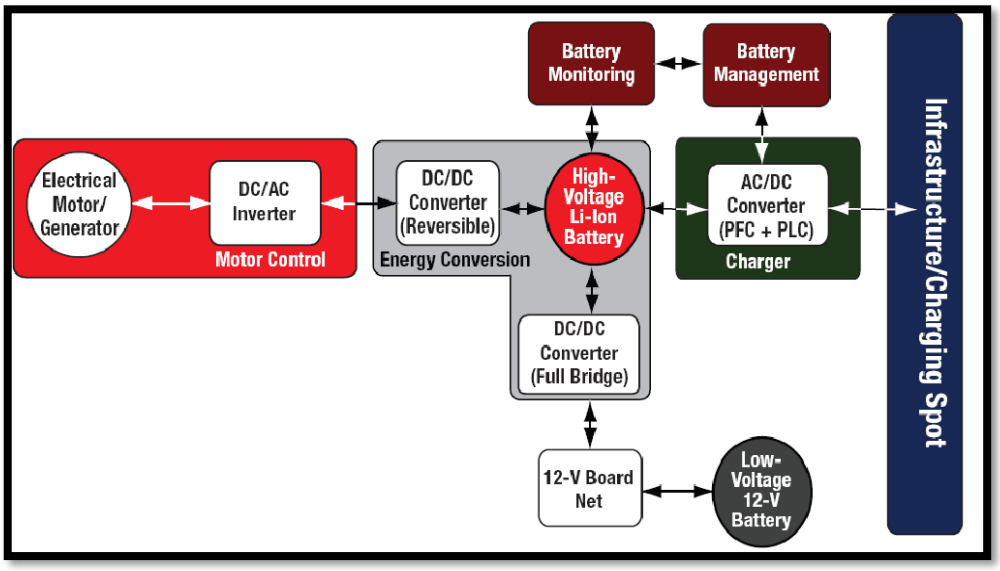

Fig.1.5: System architecture of EV/HEV

1.2 Common Battery Charging Profiles

Battery is an apparatus that directly transforms chemical energy into the electrical energy and it functions as an electrochemical cell or a pack of these cells, having the capability of accommodating the chemical energy. When it comes to vehicles, batteries are highly desirable, with traction batteries being the most common in use by electric vehicle (EV) manufacturers. These Traction batteries encompass various types such as Nickel-Cadmium, Lead Acid, Lithium-ion/polymer, Nickel-Zinc and Sodium-Nickel Chloride. To be suitable for use in EVs and plug-in hybrid electric vehicles (PHEVs), batteries must satisfy some important condition in terms of density of energy, power density, cycle life & safety. Consequently, in 2006, the USABC (US Advanced Battery Consortium) & EESTT (Electrochemical Energy Storage Technical Team) teamed up to establish the end-of-life PHEV battery requirements [8].

Ideally, EV batteries should provide a high level of autonomy, allowing the vehicle to cover a significant distance on a single battery discharge. They should also possess high specific energy and specific power, which means they should be lightweight, compact, & have the capability to store and delivering substantial amounts of power & energy, respectively. Moreover, these batteries must have longer lifespan, enduring numerous charge and discharge cycles without significant performance deterioration, while also recharging in the shortest possible time. They need to operate effectively across a wide range of temperatures, ensure safety in handling, and be recyclable with minimal cost.

Unlike batteries which are used in low-energy or low-power applications, these EV batteries need special attention to safety due to frequent fast discharge/charge cycles & the delivery of high power, which can generate excessive heat. Advance thermal management techniques & cell balancing, along with selecting appropriate battery chemistry, are important factors that impact losses in cells. One solution is the use of phase change materials, that effectively eliminate heat through the latent heat of fusion [9].

1.3 Charging Profile & Charging Infrastructures of Lithium-ion Batteries

Table 1.1: Power levels of charging (Based on [10] in part)

Charging level	Charging Power	Power supply	Charging Infrastructure's Cost (in $)	For 1hr. of charge (Range in Miles)	Charging Time	
					PHEV (in hrs.)	EV (in hrs.)
Level 1	1.40 kW @ 12 amps	120 V_{AC} Single Phase	500-800	3~4	~7	~17
Level 2	3.30 kW (onboard)	240 V_{AC} 1-Phase(Up to 80 amperes)	3,150-5,100	8~10	~3	~7
	6.60 kW (onboard)			17~20	~1.4	~3.5
Level 3	>50.0 kW (Off board)	3 phase 208 V_{AC} or 220 ~ 450 V_{DC} (~200 amps)	30,000-160,000	50~60 (80% per 0.5hrs. charge)	~0.16	0.5~0.75

The charging of PHEVs & EVs can be classified into 3 levels dependent on the power level and the specific charging infrastructure needed, as presented in Table 1.1.

1.3.1 Power Levels of Charging

In US, level 1 charging is utilized through a 1-ϕ 120 Volts/12 Amps, 60 Hz grid. Level 1 chargers can be easily integrated onboard the vehicle. The estimated cost of installing charging infrastructure of level 1 ranges from $500 to $800 [11], [12]. Level 1 charging is appropriate for home charging because it is reasonably inexpensive. However, the lower charging power results in longer charging times for the battery pack. It can take approximately 17 hrs for fully charging a 25 kWh of battery pack, starting from a 20% SOC (state of charge) to reach full SOC.

In order to charge at level 2, a 240 V outlet is needed, which is commonly found in residential garages and public facilities. Compared to level 1 charging, level 2 charging significantly reduces the charging time while still maintaining convenient accessibility. The installation cost, which includes the residential EVSE (Electric

Vehicle Supply Equipment) part, is projected to range from $3,200 to $5,200 [13]. As a result, charging of level 2 is anticipated for being the prevailing charging method for both private & public locations [3].

DC fast charging, also known as Level 3 offers significantly higher charging power, exceeding 50 kW. As a result, charging time is greatly decreased. Charging station of level 3 is expected for charging an electric vehicle upto 50% state of charge (SOC) in approximately 20 minutes. Notably, Tesla, a pioneering EV company, aims to fully charge its EVs in just 5 minutes using its supercharging stations in the near future [14], [15]. At the same time, charging of level 3 has considerable costs, including infrastructure, installation, and maintenance expenses [16], [17]. It is important to note that power delivery rapidly to a pack of battery can lead to overheating & damage cells of the battery. Additionally, sketching extra-high power from grid enhances demand & may pose overload issues for local distribution of facilities [18]– [20]. Consequently, charging of level 3 is primarily considered for public & commercial stations of charging [20]-[22].

1.3.2 Swapping of Battery

Rather than charging the pack of battery for the whole night at home, an alternative approach involves the swift replacement of a depleted battery pack with a fully charged one, allowing the driver to resume their journey promptly. This concept is known as battery swapping. In 2013, Tesla reported a battery swapping time of just 90 seconds, which is even faster than refuelling car at a gas station [23]. Swapping of battery is regarded as a promising technique that addresses the limitations of relatively slower charging of battery speeds [24], [25]. However, the current swapping of battery method is so much specific and not universally applicable to different electric vehicle models and battery types. It is necessary to establish and implement universal battery swapping standards or codes before this technique can be widely adopted in the market commercially.

1.3.3 Battery's Charging Profile

Table 1.2 presents the charging features & infrastructure details of popular EVs & PHEVs which are currently available at market. All the EVs & PHEVs listed below are provided with OBC_S that are suitable with both the levels of charging, i.e., level 1 and level 2 charging. SAE J1772 standard is addressed with of Tesla Model S having the exception, all EVs and PHEVs utilize a universal charge connector.

Table 1.2: Charging infrastructures & characteristics of some of the manufactured EVs & PHEVs

Vehicle	EV type	Battery (in kWh Li-ion)	Price (in $)	E-Rang (in mi)	Onboard Charger (in kWOBC)	Connector Type	Charging Time (in hrs.)	
							Level 1	Level 2
Mitsu-bishiI	EV	16	29,125	62	3.3	SAE J1772 JARI/TEPCO	13	4~5
BWM Active	EV	32	Lease only	100	7.2	SAE J1772	8-10	4-5
Honda Fit	EV	20	Lease only	76	3.3	SAE J1772	6	3
Chevy Volt	PHEV	16	39,145	35	3.3	SAE J1772	10	4
Honda Fit	EV	20	Lease only	76	3.3	SAE J1772	6	3
Cadillac ELR	PHEV	16.5	n/a	35	3.3	SAE J1772	n/a	4.5
Nissan leaf	EV	24	35,200	100	3.3	SAE J1772 JARI/TEPCO	22	8
Ford Focus	EV	23	39,200	76	6.6	SAE J1772	20	3-4
Tesla Model S	EV	85	95,400	265	10	Mobile Connector	34	14

*Data specified above is subject to change as it's based on the public information

Compared to other battery chemistries such as nickel cadmium, lead acid, and nickel-metal hydride, Li-ion cells exhibit significantly higher energy density [26]. In EVs and PHEVs, the energy density and weight of the battery are crucial factors which

determines range of the electric vehicles. As a result, Li-ion cells have become the dominant choice in market for PHEVs and EVs. This trend is evident from Table 1.2, where all listed PHEVs & EVs are equipped with the packs of Li-ion battery. However, it is important to note that despite advancements in battery technology leading to increased energy density, extended life cycles, and some cost reductions [4], the Li-ion battery packs remain the heaviest and costliest component in PHEVs and EVs.

There are several methods available for safely charging Li-ion batteries. The level of power at which any cell can accept the charge is not solely considered by the chemistry of the battery, but also by the charging method employed. One commonly used technique, depicted in Figure 1.6(b), is known as constant current - constant voltage (CC-CV) charging. Concept behind this approach is to charge the battery with steady maximum current, which is specified by the manufacturer of cell, until it reaches cut-off voltage. Subsequently, the voltage is held constant while the battery continues to charge until current drawn reduces to approximately one-tenth of maximum current or less, indicating that it's fully charged [27].

To enhance the battery's rate of charge acceptance, a multi-stage constant current-constant voltage (MCC-CV) charging method can be proposed [28]. The working principle of MCC-CV is similar to CC-CV, but instead of applying a single constant level of current, multiple steps of current are utilized up to the cut-off voltage, which is illustrated in Figure 1.6(a).

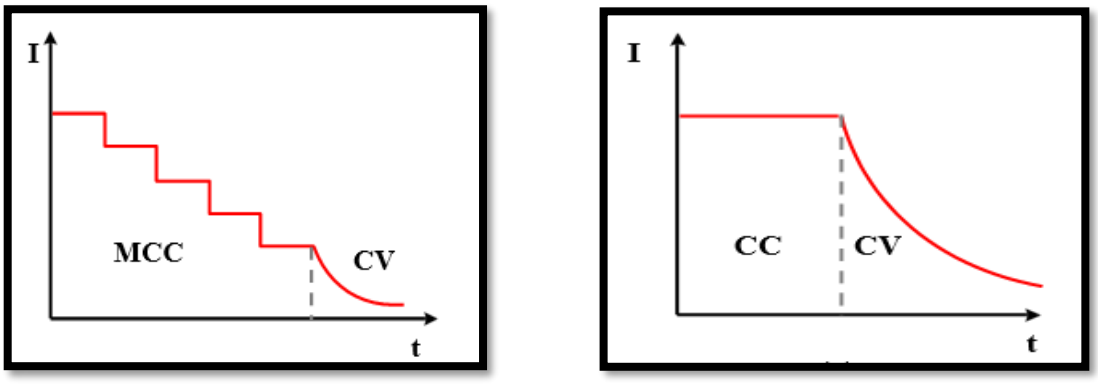

(a) **(b)**

Fig. 1.6: The charging techniques of Li-ion battery, (a) multistage constant current-constant voltage, (b) constant current-constant voltage.

The charging methods discussed above have limitations in power transfer capacity due to effects of polarization, that include electrochemical polarization, ohm polarization & consistency polarization. To overcome these limitations and improve the rate of charge acceptance, researchers are actively exploring new charging methods. One such approach, described in [25], involves discharging of battery at particular intervals of time during the charging process. This method can be implemented for both the techniques CC-CV & MCC-CV to achieve enhanced performance. Figure 1.7(b) illustrates the example of the CC-CV method with the negative pulses.

Another approach, which is proposed in [28], employs the varying pulse charge strategy. The method continuously determines the optimum pulse charge frequency for ensuring even distribution of ions in electrolyte solution. Between pulses, varying rest periods are applied to allow for ion neutralization and diffusion. The duration of this rest period is determined in real-time using a MPPT (Maximum Power Point Tracker), which identifies the maximum current acceptance level for a given state of charge (SOC). Figure 1.7(a) depicts the waveform of variable frequency connected to pulse charging. By utilizing this method, rate of charge can be enhanced in comparision to standard CC-CV & constant frequency of pulse charging methods.

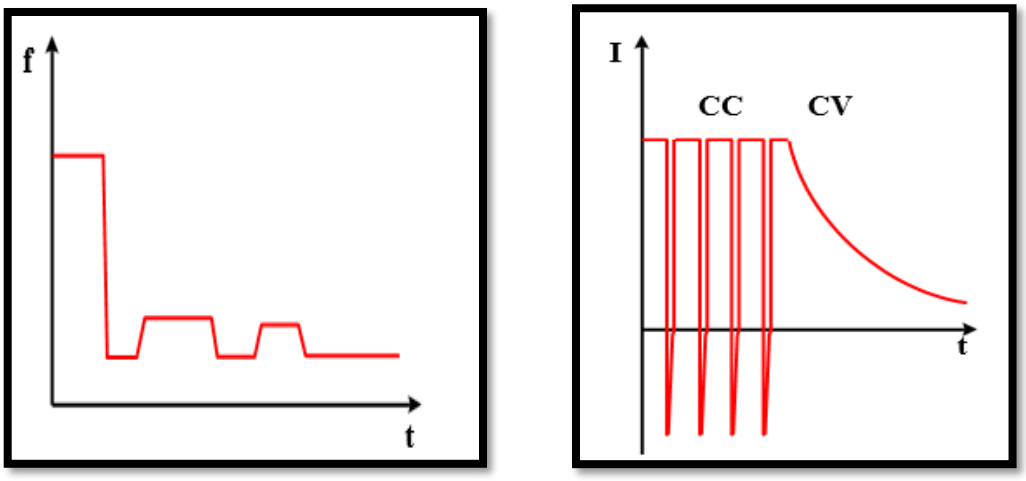

(a) **(b)**

Fig. 1.7: Advanced fast charging techniques, variable frequency pulse charge, (b) constant current –constant voltage withnegative pulse [29].

1.4 Typical Interfaces of Power Conversion & Energy Storage of EVs

The architecture of power of EV is illustrated in Figure 1.8. It consists of high voltage range (300 ~ 420) V & energy of higher range (tens of kWh) pack of battery that serves as the primary accomodation of energy unit onboard. Additionally, there are 3 key PEIs which are responsible for various power conversions. These interfaces include:

a) PEI for electric propulsion, which handles the delivery of power from pack of battery to electric motor(s) responsible for propelling the vehicle.

b) PEI for onboard appliances, which manages the power supply to various electrical systems and devices within the vehicle, such as lights, infotainment systems, and climate control.

c) PEI for onboard charging, which facilitates the charging process of battery pack by converting the external AC power from the charging station or outlet to the appropriate DC voltage and current required for battery charging.

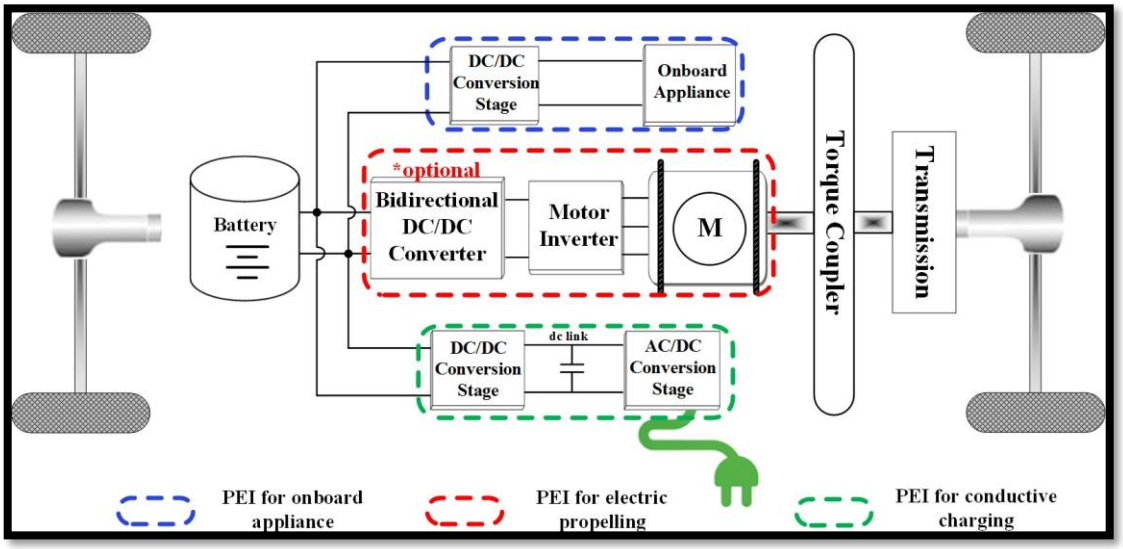

Fig. 1.8: Architecture of power for an EV.

The power electronic interface (PEI) responsible for electric propulsion comprises a bidirectional DC/DC converter & a motor inverter. This interface operates in two modes: regenerative braking mode & propelling mode. In the propelling mode,

power is transferred to the electric machine from the pack of battery, which drives the vehicle. On the other hand, in regenerative braking mode, the electric machine acts as generator, which converts the KE from braking into electrical energy. This recovered energy is then given back into pack of battery. The motor inverter serves as a rectifier during operation, ensuring the proper conversion of electrical power between the packs of batteries & electric machine. Additionally, an optional bidirectional DC/DC converter can be included in this interface to enable control over the discharging & charging processes of battery pack, enhancing the functionality of the PEI for electric propulsion [30].

The power electronic interface (PEI) dedicated to onboard appliances primarily consists of a DC/DC converter. This converter serves the purpose of reducing the high voltage provided by the battery pack (ranging from 300 V to 400 V) to a lower voltage of 12 V. The reduced voltage is then utilized to power various onboard electric appliances, including but not limited to air conditioning systems, headlights, and stereo systems. It is essential for this DC/DC converter to incorporate galvanic isolation. This feature ensures that the low voltage electronic system remains protected from any potential risks associated with the high voltage source. Galvanic isolation helps prevent hazards such as electrical shocks and allows for the safe and efficient operation of the onboard appliances [31].

The power electronic interface (PEI) for the onboard charger is responsible for transferring power from grid to charge vehicle's pack of battery. Conventionally, the onboard charger consists of 2 stages to facilitate the charging process. The first stage being responsible for converting AC from grid to DC current while ensuring power factor correction. This stage ensures efficient power conversion and improves the power quality. The second stage involves DC-to-DC conversion & provides galvanic isolation, which ensures electrical safety during the charging process [3]. Currently, commercial onboard chargers have a unidirectional flow of power, allowing power to flow from the grid to the vehicle's battery pack. However, with the emerging concept of vehicle-to-grid (V2G) technology, its suggested that batteries could also be utilized to enable flow of power from vehicle back to the power grid. That would allow the vehicle's battery to provide power to the grid when the vehicle isn’t in use, such as when it is parked. As a result, bidirectional power flow capability is required for onboard chargers in V2G applications [32]. In this V2G scenario, onboard chargers

play a crucial role in facilitating the bidirectional power flow. They enable the battery to give power back to grid when the vehicle is idle, contributing to grid stability and potentially offering economic benefits to vehicle owners. This emerging technology holds promise for future energy management strategies and grid integration [33]-[36].

1.5 Charger Classifications

Over the course of the development of electric vehicles (EVs), numerous charging systems have been proposed. These charging systems vary in terms of their configurations, necessitating a classification based on shared design & application characteristics. Table 1.3 [37] presents 5 distinct methods for categorizing chargers.

Table1.3: Battery charger's Classification

Type of Classification	**Options**
Location	Off-board, On-board
Electrical waveform	AC, DC
Power level	Level1, Level2, Level3
Topology	Dedicated, Integrated
Connection type	Mechanical, Inductive, Conductive
Power flow direction	Bidirectional, Unidirectional

Chargers can be categorized based on their circuit topologies [38]. In one approach, classification pertains to the placement of the charger. Integrating the charger on-board significantly enhances the accessibility of charging for vehicle. At the same time, on other hand, the off-board chargers have the advantage of utilizing higher amperage circuits, enabling faster charging of the vehicle within a considerably reduced timeframe.

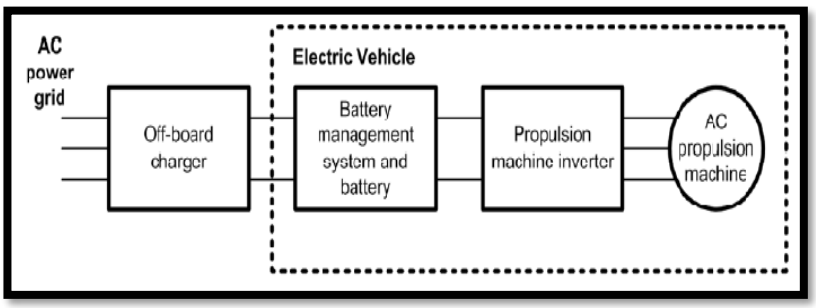

Fig.1.9: Block diagram of off-board charger

In the case of an off-board charger depicted in Figure 1.9 [38], the charger functions as an external unit separate from the EV itself. Additionally, this type of charger generates a high DC voltage that the internal BMS should be capable of handling in order to charge the battery. The main limitation of the topology is that the charger isn't integrated within the EV, which means that it's not possible to charge EV's battery without a suitable charger that can supply the required high on-site DC voltage.

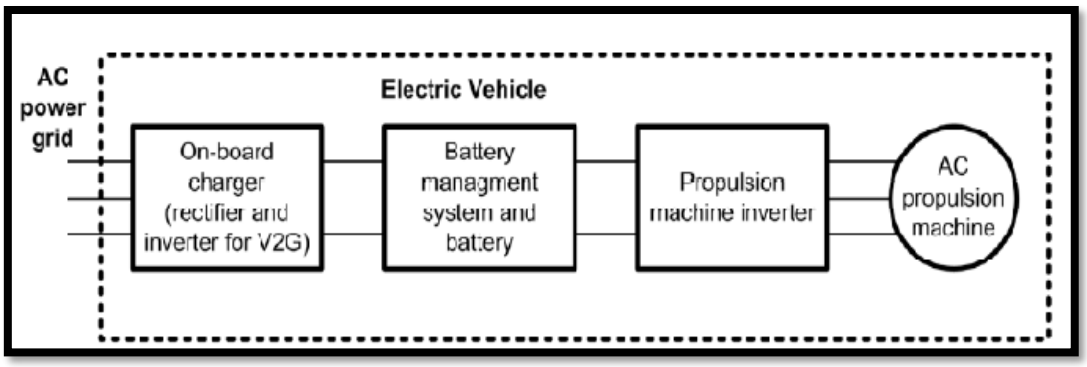

Fig.1.10: Block diagram of on-board charger

In the case of an on-board charger depicted in Figure 1.10 [38], the charger is an integral part of the EV itself. This design allows the EV to be charged using either a 1-ϕ or 3-ϕ power supply, providing charging convenience in various locations. However, a notable drawback of the topology is that the straightforward on-board charger necessitates an additional DC/AC inverter. This additional inverter serves two purposes: enabling V2G(vehicle-to-grid) capacity and driving the AC propulsion machine.

The second classification is based on electrical waveforms at connection ports between the vehicle and the grid [37]. Currently, most PHEVs & EVs available in the market utilize an AC type of connection. However, with the potential future changes in the availability & prevalence of DC sources, the connection type may also evolve.

In the third classification, 3 charging levels have been established for EVs and PHEVs, as outlined in Table 1.4 [41]. Level 1 and level 2 charging are considered the standard charging levels for locations where the vehicle will remain parked for an extended period, such as homes or offices [42]. However, the drawback of using these standard charging levels that depending on the battery size, available power, and state of charge (SOC), it may take several hours (4 to 20 hours) [43]. This extended charging time is not practical for long-distance travel. To address this issue, level 3 fast charging

was introduced. Level 3 charging significantly reduces the charging time to less than 40 minutes, making battery-powered vehicles more competitive with conventional internal combustion engine (ICE) vehicles [44]. Typically, level 3 charging is achieved through an off-board charger that transforms 3-ϕ 480-V AC power to regulated DC power. Although there are no universally adopted standards for the charging of level 3 outside of Japan [46], the Japanese CHAdeMO protocol [47] has gained international recognition. CHAdeMO enables the vehicle to receive regulated DC voltage through the external charging station, which is directly interfacing with the vehicle's battery and BMS. Alternatively, some European automakers are exploring the approach of supplying EVs directly with 3-ϕ power & processing it using an on-board battery charger [48].

Table 1.4: Charging levels of Battery

	AC Voltage (in V)	**Max. Current (in Amp)**	**Max. Power (in kW)**
Level 1	120.0V	16.0A	1.92kW
Level 2	240.0V	80.0A	19.20kW
Level 3	(300-600) V	400.0A	240.0kW

In fourth approach, a dedicated circuit is specifically designed for the intention of charging battery. Conversely, in the integral/integrated charger option, the traction inverter drive can fulfil the role of a charger while the vehicle isn’t in use and connected to grid for the charging.

The fifth classification is based on the connection method [39]. Conductive charging includes the direct metal-to-metal contact between charging infrastructure & the vehicle. On the other hand, Inductive charging utilizes a high-frequency transformer to establish an indirect connection between the AC grid & the vehicle. Lastly, mechanical charging involves the replacement of a depleted pack of battery with a fully charged one at battery swap stations.

The last classification criterion for chargers pertains to the direction of power transfer. Traditional chargers operate in a unidirectional manner, solely charging the vehicle's battery. However, more advanced charger designs have emerged that enable bidirectional power transfer [40]. It should be noted that currently, all chargers available in the market are unidirectional.

1.6 Challenges in On-board charger design

Usually, the front-end PFC stage is designed to be versatile and applicable to various charging applications. On the other hand, the second-stage converter is responsible for regulating the charger's voltage on the output side and current to accommodate different state of charges (SOCs) of the battery. This dissertation specifically concentrates on investigating both front-end PFC converter & the second-stage converter.

Table 1.5 presents a summary of the technical targets set by the U.S. DOE (Department of Energy) for a rating of 3.30 kW of level 2 onboard chargers.

Table 1.5: Technical targets of DOE on onboard charger [49]

3.30 kW Charger				
Year	Cost (in $)	Size (in liters)	Weight (in kg)	Efficiency (in %)
2010	900-$1,000	6-9	9-12	90-92
2015	600	4	4	93
2022	330	3.5	3.5	94

When designing an onboard charging interface that is both ultra-compact and highly efficient, several factors need to be considered:

1) A higher switching frequency is preferred to minimize size & weight of the system.

2) The charging interface should be capable of both step-up & step-down operations to meet the requirements of wide range of output voltage.

3) The inclusion of zero-voltage-switching (ZVS) characteristic is advantageous as it helps to minimize switching losses and mitigate high-frequency electromagnetic interference (EMI).

4) To ensure galvanic separation without sacrificing the weight and size, it is essential to integrate a high-frequency transformer into the design.

5) Efficiency optimization is crucial across the entire range of battery voltages and various load conditions to ensure optimal conversion efficiency.

Nevertheless, it presents a difficult undertaking to concurrently fulfill all the aforementioned considerations. Illustrated in Figure 1.11, an increased switching frequency corresponds to a reduced volt-sec exercised to magnetic component. Consequently, this leads to a decrease in the related core losses. But both switching loss & core loss experience an increase as the frequency rises. As a result, a higher switching frequency results in a degradation of conversion efficiency.

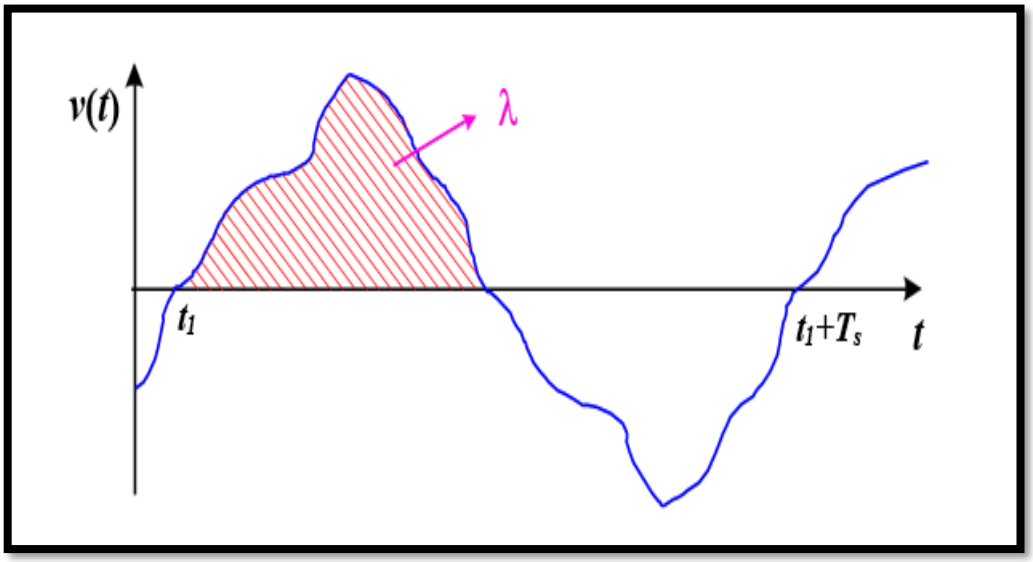

Fig. 1.11: A representation of arbitrary waveforms for the primary voltage of a transformer, demonstrating the volt-sec exercised specifically during positive phase of cycle [49].

In applications with high switching frequencies, the MOSFET is the preferred choice because of absence of tail current & its rapid speed of switching. In the hard switching configurations, increasing the switching frequencies can result in elevated stress & EMI(Electro Magnetic Interference) noise levels. Consequently, soft switching techniques like ZCS & ZVS are sought after. Among these techniques, ZVS is particularly well-suited for MOSFETs because it eliminates both the switching losses induced by semiconductor output capacitances and reverse recovery of body diode [49]. Nevertheless, the implementation of ZVS technique may give rise to high conduction losses and increased circulating current. Furthermore, in certain specific topologies like the phase shifted full bridge converter, although ZVS operation can be achieved under full load conditions, the MOSFETs present in the lagging leg may lose their ZVS characteristics when subjected to light load conditions.

An additional obstacle arises from the substantial voltage fluctuation in high

voltage pack of battery utilized in electric vehicles (EVs). With respect to the state of charge (SOC) being depleted or fully charged, the battery pack voltage varies between cut-off voltage and charge voltage (for example, 320V - 420V). Consequently, dc/dc converter stage should possess the capability to adapt to these wide range of voltages. PWM (Pulse-Width Modulation) topologies offer the advantage of easily regulating the voltage at the output within a broad range. At the same time, they suffer from the drawback of having an incomplete ZVS range. On the other hand, frequency-modulated resonant topologies provide a complete ZVS range. Nonetheless, the resonant topology's efficiency can only be optimized for specific output voltage values.

To surmount these problems onboard charging system that is exceptionally compact and exhibits high efficiency, attention must be given to the following components and technologies:

1) Enhanced magnetic materials: The dimensions of magnetic parts are limited by core losses linked to the high switching frequency. To address this issue, it is necessary to incorporate more advanced magnetic materials that exhibit reduced core loss at higher switching frequencies.

2) Enhanced packaging techniques: The packaging of the onboard charging system plays a crucial role in determining its size. Employing advanced packaging techniques enables enhanced utilization of space and improved dissipation of heat.

3) Enhanced cooling techniques: Heat sinks account for a significant portion of the volume occupied by charging systems. The heat sink's size is directly influenced by cooling techniques employed. In general, active method of cooling is superior to passive method of cooling. Liquid method of cooling is typically preferred for conventional power electronic interfaces based on Silicon.

4) Enhanced switching power devices: A significant part of total system losses can be attributed to power losses arising from switching power devices like diodes & MOSFETs. Utilizing advanced power devices that feature high voltage ratings, low on resistances, high operating temperature and faster

switching speeds capabilities can effectively mitigate power losses and alleviate thermal stress within the system.

5) Enhanced control methods and converter topologies: The performance characteristics of a circuit, including features like EMI, conduction losses, ZVS, circulating current, and switching losses, are heavily influenced by the converter topology. Employing optimized ckt topologies & control methodologies can greatly enhance overall efficiency of the circuit across a wide range of battery SOC (State of Charge).

1.7 Charger System

The duration it takes to charge a battery and its overall lifespan are greatly influenced by the specific attributes of the battery charger [50]-[52]. Numerous manufacturers globally are currently engaged in developing diverse modules of battery for hybrid & electric vehicles. The effectiveness of these modules of battery relies not only on their design but also relies on how they are charged & utilized. In this context, battery charger plays a very crucial role in the advancement of these technologies**.**

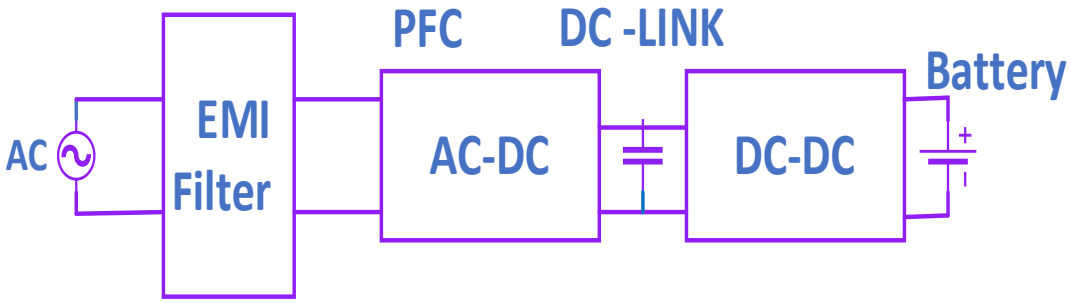

Fig.1.12: Battery charger system

Figure 1.12 [53] illustrates the conventional configuration of a battery charger system. Given that batteries possess a limited energy capacity, PHEVs & BEVs require periodic recharging, conventionally by connecting them to the AC mains supply. The charging infrastructure for above vehicles comprises a rectifier, which transforms the line voltage which is AC into a DC, followed by DC/DC converter which generates the necessary DC voltage for the pack of battery. In some cases, advanced charging systems may also utilize PLC (Power Line Communication) modems to establish communication with the power grid, enabling adjustments to the

charging process based on power grid conditions. To optimize energy utilization and extend battery life, it is crucial to closely monitor the battery pack during operation and charging.

1.8 Motivation

This thesis focuses on how to design & model an on-board battery charger for EVs which has the capability of efficiency optimization over a wide battery voltage range. The major aim of this research is to enhance the quality of power at the supply side of converters by ample amount of work in the following domains:

1) Performed an extensive review of the existing literature on onboard charging for Plug-in Electric Vehicles (PEVs).
2) We introduced a novel approach to assess the charging performance of resonant topologies in a more effective manner.
3) Two stage converter is implemented where PFC converter is the 1st stage & the Half Bridge LLC Resonant Converter is used as the 2nd stage.
4) Boost Converter and SEPIC are used as the first stage PFC converter and their respective performances are analysed.
5) Analysing the issue of significant inrush current in boost topologies and have identified a potential solution to address this problem.

1.9 Thesis Outlines

The thesis is classified into 5 chapters. The synopsis of every chapter is listed below:

Chapter 1 deals with the background of EVs, different charging profiles and charging infrastructures. EV Charger needs are extensively described along with the classification of charging and the challenges related to on board charging are also discussed along with the motivation behind this work.

Chapter 2 presents the literature survey, where the learnings from different sources and authors have been discussed.

Chapter 3 discusses about the basic resonant converters along with it's classifications.

Chapter 4 introduces a configuration that combines a boost converter and an LLC resonant converter. The boost converter is employed for PFC, while the LLC resonant converter is responsible for facilitating the battery charging.

Chapter 5 discusses the utilization of a SEPIC to power a half-bridge LLC resonant converter for battery charging. The SEPIC addresses the issue of significant inrush current that typically arises in boost converters. The half-bridge LLC resonant converter is then employed specifically for the purpose of charging the battery**.**

Chapter 6 describes the summary of this research upon on-board charging of Electric Vehicle battery and at the same time also discusses the scopes which are there in future for this research work

CHAPTER 2

LITERATURE REVIEW

2.1 Literature Review on On-board Electric Vehicle Charger

a) **Khaligh & S. Dusmez (2012),** This paper offers a thorough examination of the various topological aspects related to both inductive and conductive charging solutions designed for plug-in electric vehicles. along with the Electric Vehicles [EVs] battery charging applications. According to this the two-stage isolated AC/DC converters are the most commonly used topologies now a days [78].

b) **C.-Y. Oh et. al. (2013),** this paper gives ideas on a high-efficient non-isolated single-stage on-board battery charger for EVs [79]. According to this paper the most commonly used topology in the electric vehicle's charger is the boost-type DC-DC converter because of it has the following features:

   i. simple circuit configurations,
   ii. lower number of components,
   iii. lower THD, &
   iv. continuous input current.

c) **H.-S. Kim et. al. (2013),** this paper describes about the high-efficiency isolated bidirectional AC–DC converter for a DC distribution system. According to this paper the DC–Link voltage i.e., the input voltage for the second stage is usually regulated at 390V to be compatible with the general grid voltage which is in the range of 85V-265V [80].

d) **F. Musavi et. al. (2013),** This paper presents ideas about an LLC resonant DC–DC converter for wide output voltage range battery charging applications and also gives the same information as the above research that the DC–Link voltage i.e., the input voltage for the second stage is usually regulated at 390V to be compatible with the general grid voltage (85V-265V) [81].

e) **B. Gu et. al. (2013),** This research study focuses on the analysis of a zero voltage-switching PWM Resonant Full-Bridge converter for electric vehicle battery chargers. The study specifically addresses the reduction of circulating losses and minimization of voltage stresses on Bridge Rectifiers [82] and it is

shown that the LLC resonant converters are typically used because of their following attractive features:

i. low Electromagnetic Interference (EMI),
ii. minimal size,
iii. high-frequency operation,
iv. soft switching,
v. short circuit protection, and
vi. galvanic isolation

f) H. Wang & F. Blaabjerg (2014), in this study an overview on reliability of capacitors for DC-link applications in power electronic converters has been done. It describes that LLC resonant converters are typically used because of their attractive features such as low Electromagnetic Interference (EMI), minimal size, high-frequency operation, soft switching, short circuit protection, and galvanic isolation [83].

g) G. Pledl et. al. (2010), This research study elucidates the operational theory, design methodology, and simulation of a bidirectional LLC resonant converter tailored for vehicular applications which tells that LLC resonant converter to control its output voltage and operation at resonance frequency as the optimal operating frequency to achieve the highest efficiency [84].

h) R. Pandey & B. Singh (2011), this study gives the ideas about a Power Factor Corrected LLC resonant converter for electric vehicle charger using cuk converter, which gives the information that the peak efficiency of a conventional battery charger with PFC based on the boost converter might be around 94%, but it is less efficient at medium and light loads. Boost converter also suffers from high inrush current [85].

i) R. Beiranvand et. al. (2011), this paper describes the Use of LLC Resonant Converter for the designing of voltage source with wide-range. According to it, the operating frequency of LLC resonant current decreases and moves away from the resonant frequency of the LLC resonant converter when the battery voltage is less than its nominal voltage at a lower State of Charge (SOC) which results in high switching and circulating losses in the converter and degrade the efficiency of the charger [86].

2.2 Conclusion

An on-board battery charger for EVs which has the capability of efficiency optimization over a wide battery voltage range. The most commonly used topology is the boost-type DC-DC converter because of its simpler circuit configurations, lower number of components, continuous input current & THD. The SEPIC addresses the issue of significant inrush current that typically arises in PFC boost converters. The half-bridge LLC resonant converter is employed specifically for the purpose of charging the battery**.** LLC resonant converters are typically used because of their attractive features such as low Electromagnetic Interference (EMI), minimal size, high-frequency operation, soft switching, short circuit protection, and galvanic isolation.

CHAPTER 3
BASIC RESONANT CONVERTERS

3.1 Introduction

Resonant converters, which underwent extensive research in the 1980s [54]-[61], offer the advantage of very low switching losses, making it possible for resonant topologies for operating at large switching frequencies. Among resonant topologies, the SRC (Series Resonant Converter), PRC (Parallel Resonant Converter), SRC (Series Resonant Converter), & SPRC (Series Parallel Resonant Converter which is also known as LCC resonant converter) are 3 most widely used configurations. The analysis & design of these topologies have been deeply investigated and studied**.**

3.2 Series Resonant Converter

Fig.3.1 (a) depicts the ckt. diagram of a half-bridge SRC [62]-[67], while Figure 3.1 (b) illustrates the gain curve of the SRC. In this configuration, the resonant capacitor (Cr) & resonant inductor (Lr) are connected in series, forming a resonant tank in series. This resonant tank is then connected in series with a rectifier-load network. The load & resonant tank together play a role of voltage divider. After adjusting the frequency of the Vd (driving voltage), impedance of the resonant tank changes, consequently affecting the distribution of the input voltage. Since the system operates as voltage divider, DC gain of the SRC always < 1. Under light-load conditions, where the load impedance is significantly larger than the resonant network's impedance, the entire input voltage is applied across the load. This poses a challenge in regulating the output at light loads. In theory, an infinitely high frequency would be required to regulate the output when there is no load.

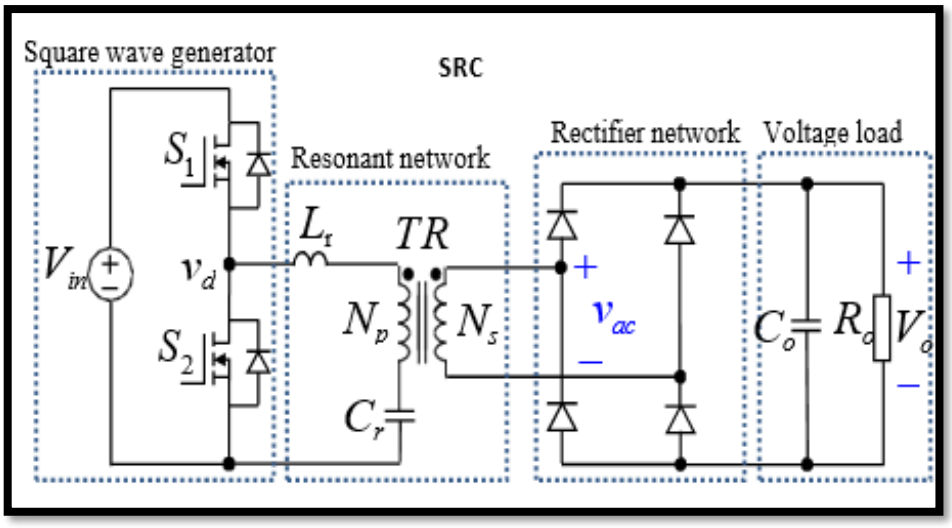

Fig.3.1(a): Configuration of the Half Bridge SRC circuit

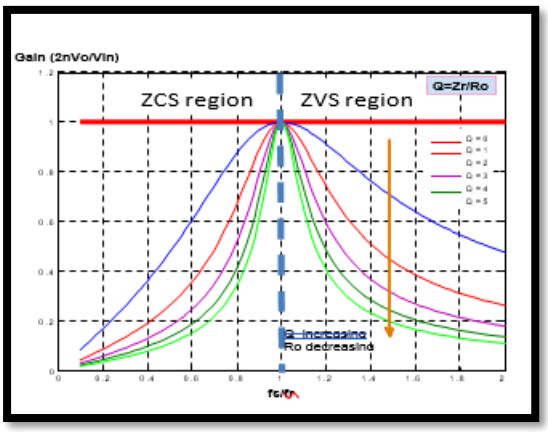

Fig.3.1(b): Gain Curves of the Half Bridge SRC

When the switching frequency of a converter is lesser than its resonant frequency, it operates in zero current switching (ZCS) conditions. Conversely, when the switching frequency exceeds the resonant frequency, the converter operates under zero voltage switching (ZVS) conditions. In the case of power MOSFETs, zero voltage switching is preferred. Examining the operating region reveals that at light loads, to maintain a output voltage which is regulated the switching frequency should be significantly increased. This poses a significant challenge for the SRC. Additional control methods must be implemented for the regulation of output voltage at light loads. As the voltage at input rises, the converter operates at higher frequencies, moving further away from the resonant frequency.

As the frequency rises, the resonant tank's impedance also increases. Consequently, instead of being transferred to the output, a larger portion of energy circulates within the resonant tank. In this case, circulating energy refers to the energy that is returned to the input source during each cycle of switching. The greater the quantity of energy given back to source in every cycle, higher will be the energy that needs to be handled by the semiconductors, resulting in increased conduction losses. Additionally, at lesser input voltages, the turn-off current is significantly lower. Conversely, the turn-off current will also increase when the voltage at input will increase.

Based on the aforementioned analysis, it is evident that the SRC faces several significant challenges, including difficulties in regulating output at light loads, dealing with high energy being circulated, and managing turn-off currents under higher input voltage conditions.

3.3 Parallel Resonant Converter

Figure 3.2 (a) illustrates the schematic of a parallel resonant converter [68]-[71], while Figure 3.2 (b) displays its gain curve. In the PRC, resonant tank remains connected in series. However, it is referred to as a PRC because the load is connected in parallel with the resonant capacitor. To be precise, this converter should be referred to as a SRC with parallel load. As the primary side of the transformer is capacitive, an inductor is connected on the secondary side for impedance matching.

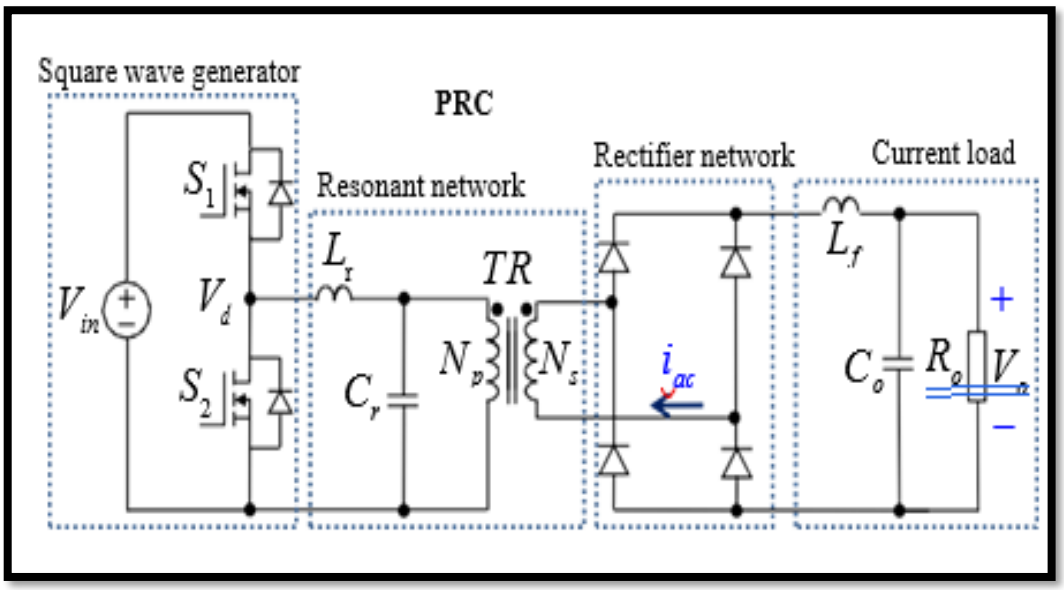

Fig.3.2 (a): Configuration of the Half Bridge PRC Circuit

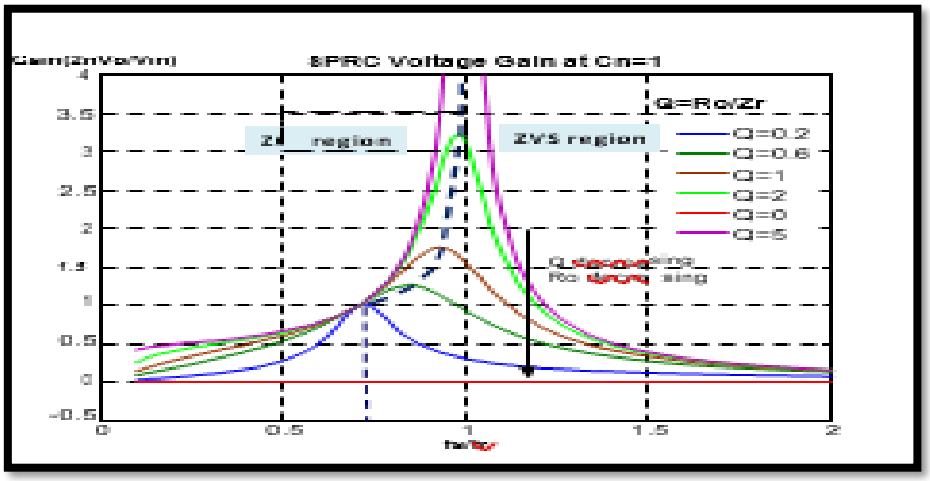

Fig.3.2(b): Gain Curve of the Half Bridge PRC Circuit

By examining the gain curves shown in Figure 1.12.(b), it can be observed that, similar to the SRC, the PRC is also designed to operate on the right side of the resonant frequency in order to achieve ZVS. However, compared to the SRC, the operating region of the PRC is relatively smaller due to a steeper curve. Remarkably, at light loads, the frequency does not need to be significantly altered to maintain a regulated output voltage. Hence, the issue of light load regulation, which exists in the SRC, does not affect the PRC. At higher input voltages, the converter operates at higher frequencies, considerably distant from the resonant frequency. Additionally, by examining the MOSFET current, it can be observed that at lower input voltages, turn-off current is notably lower.

When comparing the PRC with the SRC, it is evident that the circulating energy in the PRC is considerably higher. A significant challenge in PRC is that substantiality in the circulating energy is observed even at lighter loads. This is attributed to the fact that the resonant capacitor is connected in parallel with the load. Even under no-load conditions, the input still encounters a relatively low impedance from the series resonant tank. As a result, significant circulating energy is induced, even when the load is zero.

The primary challenges faced by the Parallel Resonant Converter (PRC) include the presence of high circulating energy and the occurrence of high turn-off currents under high input voltage conditions.

3.4 Series Parallel Resonant Converter

Figure 3.3.(a) presents the schematic of a series parallel resonant converter (SPRC) [72]-[74], while Figure 3.3.(b) displays its gain curve. The resonant tank of

the SPRC comprises 3 resonant components: Cpr, Lr, and Csr. The resonant tank in the SPRC can be viewed as a combination of the SRC and the PRC. Similar to the PRC, an inductor is connected on the secondary side for impedance matching. The SPRC combines the favourable characteristics of both the PRC and the SRC. With the load connected in series with the series tank consisting of Lr and Csr, the circulating energy in the SPRC is smaller compared to the PRC. Additionally, the parallel capacitor Cpr allows the SPRC to regulate the output voltage even under no-load conditions.

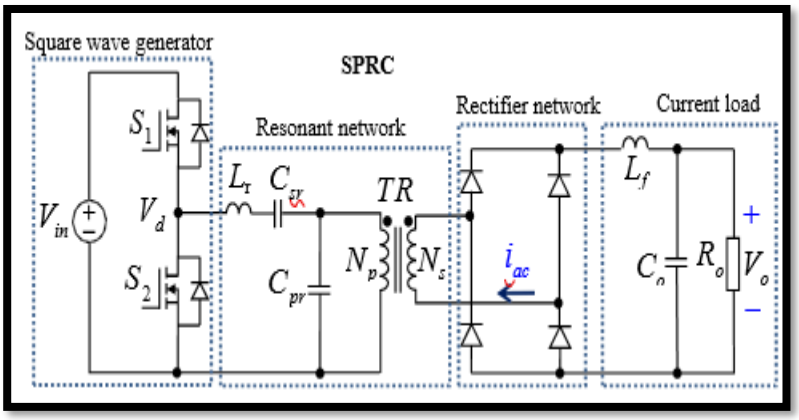

Fig.3.3(a): Configuration of the Half Bridge SPRC Circuit

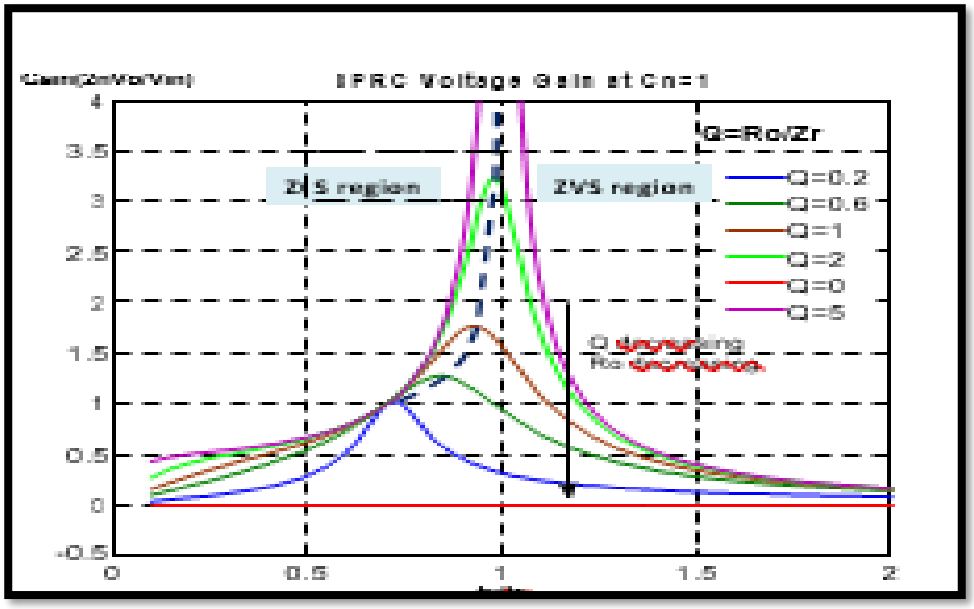

Fig.3.3(b): Gain Curve of the Half Bridge SPRC

Like the SRC and the PRC, the SPRC also designed to operate on right side of the resonant frequency for achieving ZVS. Analysing the operating region of graph

reveals that the SPRC exhibits a narrower range of switching frequencies with load variations compared to the SRC.

The input current of the Series Parallel Resonant Converter (SPRC) is significantly smaller than that of the Parallel Resonant Converter (PRC) and slightly larger than that of the Series Resonant Converter (SRC). Consequently, the circulating energy in the SPRC is reduced when compared to the PRC.

Similar to the SRC and the PRC, the SPRC operates at higher frequencies, far from the resonant frequency, when subjected to high input voltages. Furthermore, like the PRC and SRC, the SPRC experiences an increase in both circulating energy and MOSFET turn-off currents when operating at high input voltages.

Based on the aforementioned analysis, it is evident that the Series Parallel Resonant Converter (SPRC) incorporates the favourable characteristics of both the Series Resonant Converter (SRC) and the Parallel Resonant Converter (PRC). It exhibits reduced circulating energy and displays less sensitivity to load variations.

Regrettably, the SPRC continues to face significant challenges when designed for wide input voltage ranges. In such scenarios, the converter experiences a considerable penalty, with increased switching loss & conduction at higher input voltages. The switching losses observed are similar to those encountered in Pulse Width Modulation (PWM) converters operating under high input voltage conditions.

Optimizing these three converters at high input voltages poses a challenge. Wide input ranges can lead to high conduction losses and switching losses, diminishing their overall efficiency.

3.5 LLC Resonant Converter

The 3 conventional resonant topologies discussed earlier suffer from significant drawbacks when designed for wide input voltage ranges. They experience challenges such as increased circulating energy and higher switching losses at high input voltages. Valuable insights can be derived from these analyses. It is observed that operating a resonant tank at its resonant frequency yields the most efficient results. This principle applies particularly well to the SRC and the PRC. As for the SPRC, which possesses two resonant frequencies, and operating at its highest resonant frequency generally offers better efficiency.

For achieving ZVS, the converter must operate on the DC characteristic's negative slope. However, similar to the SRC and the PRC, the SPRC also faces challenges in optimizing its performance for high input voltages. This is due to the converter operating at switching frequencies that are far from the resonant frequency under such conditions. Analysing the DC characteristic of the SPRC reveals the existence of two resonant frequencies: a lower resonant frequency which is determined by the series resonant tank comprising Csr & Lr, and a higher resonant frequency which is determined by Lr & the equivalent capacitance of Cpr & Csr in series. Generally, resonant converter achieves high efficiency when operated at its resonant frequency. Unfortunately, for the SPRC, even though it has 2 resonant frequencies, lower resonant frequency falls within the zero current switching (ZCS) region, making it unsuitable for designing the converter to operate at this frequency in the present application. However, the objective is to find a resonant frequency within the ZVS region. This can be achieved by configuring an LLC resonant converter, as depicted in Figure 3.4 (a) [75]-[77]. The DC characteristics of the LLC converter is the reverse of the DC characteristics of the SPRC. The LLC converter also has 2 resonant frequencies, where the higher resonant frequency is calculated by Lsr and Cr. The lower resonant frequency is calculated by the series inductance of Lsr & Lpr and Cr. Notably, the higher resonant frequency falls within the ZVS region, allowing the converter to be designed to operate around this frequency.

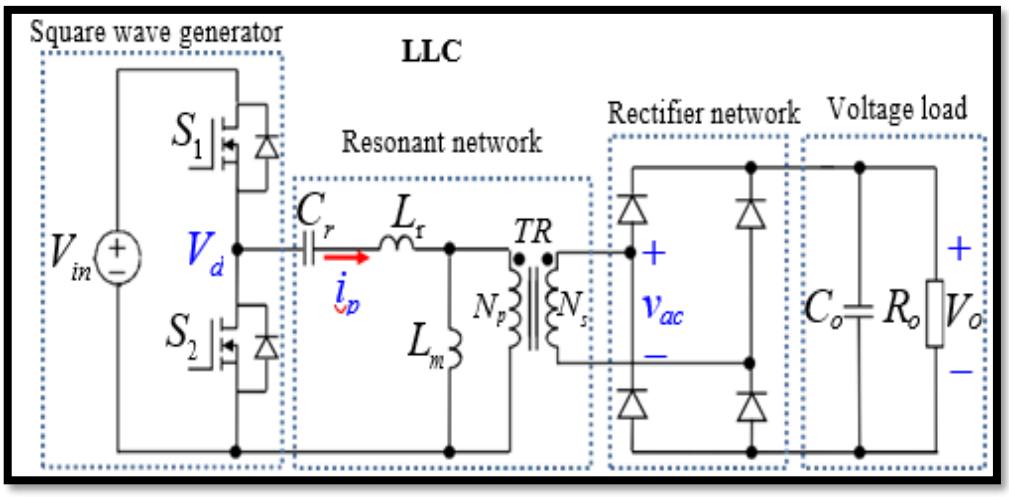

Fig.3.4(a): Circuit Configuration of HB-LLC Resonant Converter

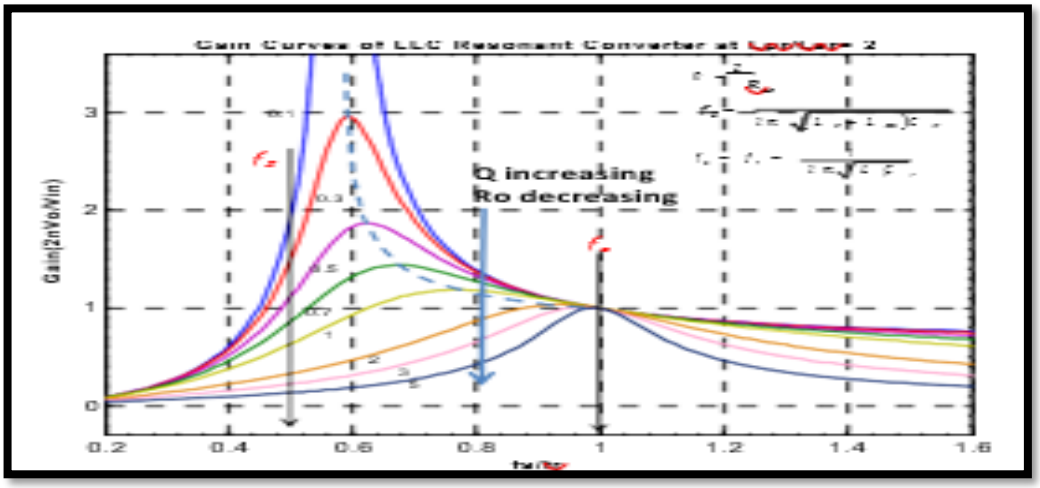

Fig.3.4(b): Gain curves of HB-LLC Resonant Converter

These 2 key features of the LLC converter can be leveraged in applications where it is employed:

(a) The LLC converter offers a narrow range of switching frequency during light load conditions and exhibits ZVS capability, even when there is no load. As a result, it enables significantly reduced switching losses, leading to high efficiency.

(b) The LLC converter possesses the ability to regulate the output voltage under varying load and line conditions.

CHAPTER 4
A BOOST PFC FED LLC RESONANT CONVERTER

4.1 Introduction

The two-stage scheme for battery charging is presented in this work. A power factor correction circuit called a diode bridge rectifier makes up the first step. The boost converter control strategy in DCM makes the PFC control algorithm simpler, but on the other hand it generates a large peak in the input current, which leads to overdesigning of the input filters. [87],[88]. The usage of equipment with lower power ratings is constrained by this. To overcome this, the input inductor current (IL1) is utilized in CCM, reducing the stress on the input current for the purpose of shaping the current. CCM is being used while DCM is capable of providing natural power factor correction without any current feedback because of low values of peak current, switching device conduction losses, turn-off losses and high-frequency ripple amplitude. Resonant half-bridge LLC converter forms the second stage that makes charging the batteries easier. Proportional-Integral (PI) controller helps in controlling the output voltage of the battery.

Fig.4.1 depicts a battery charger for an electric vehicle that employs a boost converter as the first stage and a Half-Bridge LLC resonant converter as the second stage. The boost converter is powered by an AC main supply through the Diode Bridge Rectifier (DBR). Power Factor Corrected-Boost converter functions in a state of CCM for the IL1. The APFC generates harmonic-free AC mains current and also controls DC-link voltage. The Active Power Factor Controller has a two-loop architecture, with the boost converter feedback's input inductor current (IL1) serving as the internal loop, i.e., current control loop and outer loop, i.e., voltage control loop is served by DC-link voltage. When sensing DC-link capacitor voltage (Vdc) and reference DC-link voltage (Vdc*) are compared, the outer voltage control loop structure is initiated, resulting in a voltage error. After processing the voltage error, the PI controller generates a modulating current signal. Furthermore, the product of modulating current signal and the AC mains voltage's unit template is compared to boost converters' IL1 to produce the current error signal. This error signal is then sent through the PI controller, which also serves as current controller, after that the resulting signal and the saw-tooth carrier wave are compared for generating boost converter's PWM switching pulses.

The LLC resonant DC-DC converter is used to build the second stage. V_{dc} powers this second stage converter, and PI-Controller regulates converters' output voltage (V_O). V_O and Vo_{ref} (reference output voltage) are further compared, and the PFM controller processes the resulting signal, generating the switching pulse for this second stage converter, and the Proportional-Integral Controller acting as voltage controller processes V_O.

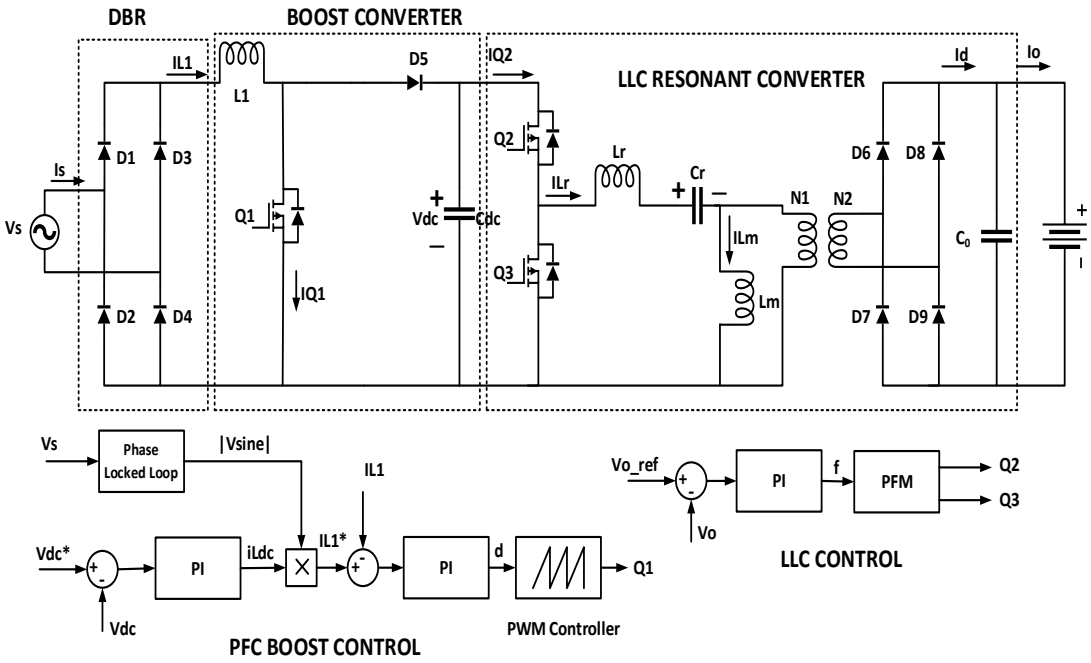

Fig.4.1: Proposed LLC Resonant Converter Control

4.2 Design of Proposed Battery Charger for Electric Vehicle

This section discusses the design of a boost PFC-based electric vehicle battery charger. The following assumptions are taken into account when determining the design parameters.

i. This proposed topology's semiconductor devices are ideal.

ii. The battery's resistance load is considered.

4.2.1 The Development of a Boost Converter with Power Factor Correction

The PFC-based boost converter is designed with active power factor control (APFC) in the input inductor's continuous conduction mode. The specification in Table 4.1.

Table 4.1: Boost Converter Specifications

Parameter	**Variable**	**Value**
Supply Voltage	V_s	220 V
Output Power	P_o	576 W
Supply Frequency	f_{supply}	50 Hz
Switching Frequency	f_{sw}	30 kHz
Input inductor current ripple	ΔI_{L1}	10 %
DC-link Voltage	V_{dc}	400 V
DC-link ripple voltage	ΔV_{dc}	1.5 %

The DBR output voltage (V_{dbr}) and V_{dc} helps in determining the duty cycle (D). Ignoring the drop across the DBR diode, D is written as follows:

$$D = \frac{V_d - V_{dbr}}{V_d} \qquad (4.1)$$

For a_i 220V supply voltage, the DBR's (Vdbr) output voltage is 198V. For this design, the 400V DC-link voltage is taken into account. Therefore, the duty cycle is determined as,

$$D = \frac{400-198}{400} = 0.50 \qquad (4.2)$$

Taking into account the calculation for 10% current ripple of the input current,

$$\Delta I_{L1} = \frac{P_o}{V_{dbr}} \times 10\% = \frac{576}{198} \times 0.1 = 0.291\ A \qquad (4.3)$$

The ripple current of 0.291A is taken into account when calculating the boost input inductor value. The input inductor has the following value:

$$L_1 = \frac{V_{dbr} \times D}{\Delta I_{L1} \times f_{sw}} = \frac{198 \times 0.50}{0.29 \times 30 \times 10^3} = 11.37\ mH \qquad (4.4)$$

Voltage ripple (ΔV_d) is set to 1.5% Vdc, for avoiding significant ripple at the DC-link. ΔV_d is expressed as,

$$\Delta V_d = \frac{1.5}{100} \times V_d = \frac{1.5 \times 400}{100} = 6V \quad (4.5)$$

The DC-link capacitor is described below using a voltage ripple of 6V:

$$C_d = \frac{P_o}{4\pi f_{supply} V_d \Delta V_{Cd}} = \frac{576}{4\pi \times 50 \times 400 \times 6} = 383\mu F \quad (4.6)$$

4.2.2 The Development of a Half-Bridge LLC Resonant Converter

Vdc is successfully regulated by the voltage controller used in the APFC as an$_i$ outside loop. This V_{dc} is delivered to the second stage. Specifications provided in Table 4.2 gives design value of LLC resonant converter's components.

Table 4.2: Half-Bridge LLC Specifications

Parameter	**Variable**	**Value**
Output Voltage	V_o	48 V
DC-link Voltage	V_{dc}	400 V
Output Power	P_o	576 W
Resonant Frequency	f_r	70kHz

Given are the battery's charge voltage of 48V, the DC link voltage of 400V, and the turns ratio (T) is specified as,

$$T = \frac{V_d}{2V_o} = \frac{400}{2 \times 48} = 4.16 \quad (4.7)$$

The transformer's turns ratio is set to 4.3 in order to operate the second stage converter below its resonant frequency(f_r). The maximum current of the LLC's resonant tank is calculated as,

$$I_{Lr} = \frac{2\pi P_o}{2V_d} = \frac{2\pi \times 576}{2 \times 400} = 4.52\ A \qquad (4.8)$$

To design the second stage converter's parameters, value of f_r is taken as 70kHz. The resonant capacitor (C_r) is given as,

$$C_r = \frac{I_{Lr}}{2\pi f_r {}^{V_d}/_2} = \frac{4.52}{2\pi \times 70 \times 10^3 \times {}^{400}/_2} = 51.4nF \qquad (4.9)$$

The Lr/Lm ratio is set to 0.167 in order to provide appropriate voltage gain to the second stage converter. We may compute resonant inductance & magnetising inductance as follows:

$$L_r = \frac{1}{(2\pi f_r)^2 C_r} = \frac{1}{(2\pi \times 70 \times 10^3)^2 \times 51.4n} = 100.6\mu H \qquad (4.10)$$

$$L_m = L_r/0.167 = 100.6\mu H/0.167 = 604\mu H \qquad (4.11)$$

4.3 Control Techniques of Proposed Charger

The Boost converter controller is made up of two loop structures. The outer voltage loop controls the DC-link voltage Vdc. The voltage error produced by the PI controller is processed by comparing it to V_{dc}*, and the resultant is specified as,

$$i_{LDC}(z) = G_{pv}\{V_e(z) - V_e(z-1)\} + i_{LDC}(z-1) + G_{pi}V_e(z) \qquad (4.12)$$

where the proportional and integral gains of the voltage controller, respectively, are denoted by Gpv and Gpi.

The reference input inductor current is obtained as follows by multiplying the voltage loop output by the input voltage sine template:

$$I_{L1}{}^*(z) = I_{L1}(z) \times v_{\text{sine}}(z) \qquad (4.13)$$

The PI controller processes the current error, and the outcome is stated:

$$d(z) = G_{pi}\{I_e(z) - I_e(z-1)\} + d(z-1) + G_{ii}I_e(z) \quad (4.14)$$

where the proportional and integral gains of the current controller, respectively, are denoted by Gpi and Gii.

The second stage LLC resonant converter employs a voltage controller and pulse frequency modulation (PFM). By comparing the V_{Oref} with the battery voltage, the Proportional-Integral controller calculates the voltage error (V_{oe}), and expresses the result as,

$$f(z) = f(z-1) + G_{pllc}\{V_{oe}(z) - V_{oe}(z-1)\} + G_{illc}V_{oe}(z) \quad (4.15)$$

where Gillc is the Half-Bridge LLC resonant converter's integral gain and Gpllc is its proportional gain.

The gains for various controllers are shown in Table 4.3.

Table 4.3: PI Gains Value

Variable	**Gain**
$\mathbf{G_{pv}}$	0.54
$\mathbf{G_{pi}}$	21.77
$\mathbf{G_{pi}}$	7.00
$\mathbf{G_{ii}}$	1300
$\mathbf{G_{pllc}}$	500
$\mathbf{G_{illc}}$	10,000

4.4 Simulation Result and Discussion

This section discusses the effectiveness of the suggested converter for charging electric vehicle batteries. By adjusting the supply input voltage and load variation, the proposed charger's dynamic and steady state performance is examined. Table 4.4 lists all of the parameters that were determined in section 4.3.

Table 4.4: Proposed Charger Parameters

Parameter	Variable	Value
Supply Voltage	V_s	220 V
Output Power	P_o	576 W
Switching Frequency	f_{sw}	30 kHz
Resonant frequency	f_r	70kHz
Supply Frequency	f_{supply}	50 Hz
DC-link Voltage	V_{dc}	400 V
DC-link Capacitor	C_d	383 μF
Input inductor	L_1	11.37 mH
Magnetizing Inductor	L_m	604 μH
Resonant Inductor	L_r	100.6 μH
Resonant Capacitor	C_r	604 μF

4.4.1 Performance at Steady-State for the PFC-Boost Converter

PFC Boost converter's steady-state performance is examined in this section using supply voltages Vs = 220V & Vdc = 400V. Rated output ratings are: Vo = 48V at Po = 576 Watt. Maximum amplitude of the sinusoidal waveform of the AC mains supply current is 4A. With a maximum current of 4A, IL1 is functioning in CCM. In figure 4.2, the IL1 waveform is shown. Vdc = 400V is effectively obtained using the Proportional-Integral Controller.

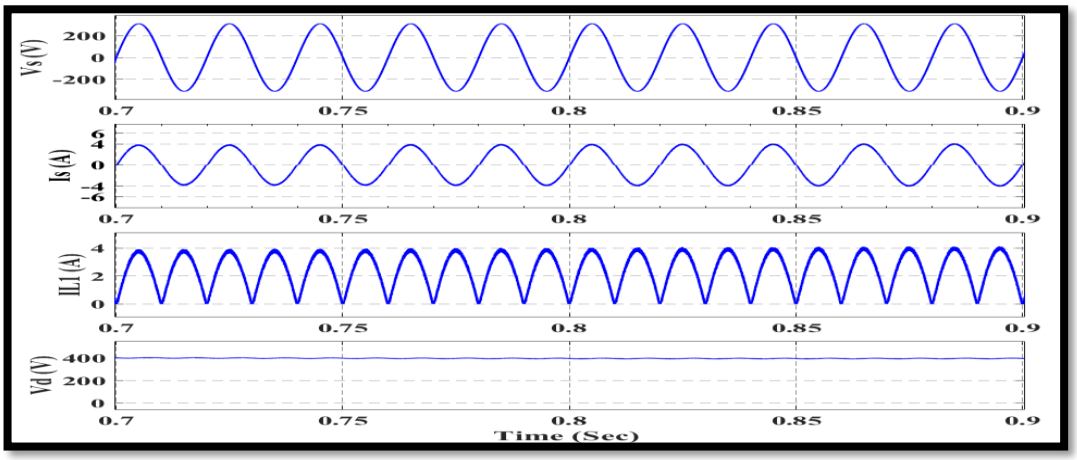

Fig.4.2: Performance for supply current (Is), DC-link voltage (Vdc) & input inductor current (IL1) under steady-state conditions at supply voltage (Vs) = 220V.

4.4.2 The LLC Resonant Converter's Steady State Performance

Here, steady-state performance of second stage converter is explored. A load current of 12A brings the battery voltage to Vo = 48V. The magnetising current's maximum amplitude, shown in figure 4.3 as ILm, is 1.2A. Resonant current has a 5.1A peak value when the current waveform is triangular. The second stage converter is operating close to fr, which is the region most suited for the converter's ideal performance, as seen by the waveforms of ILm and ILr. With a load of 576 W, the capacitor VCr can withstand a maximum voltage of 404V. The output current of rectifier (Id) is in CCM and has 21A as the maximum amplitude.

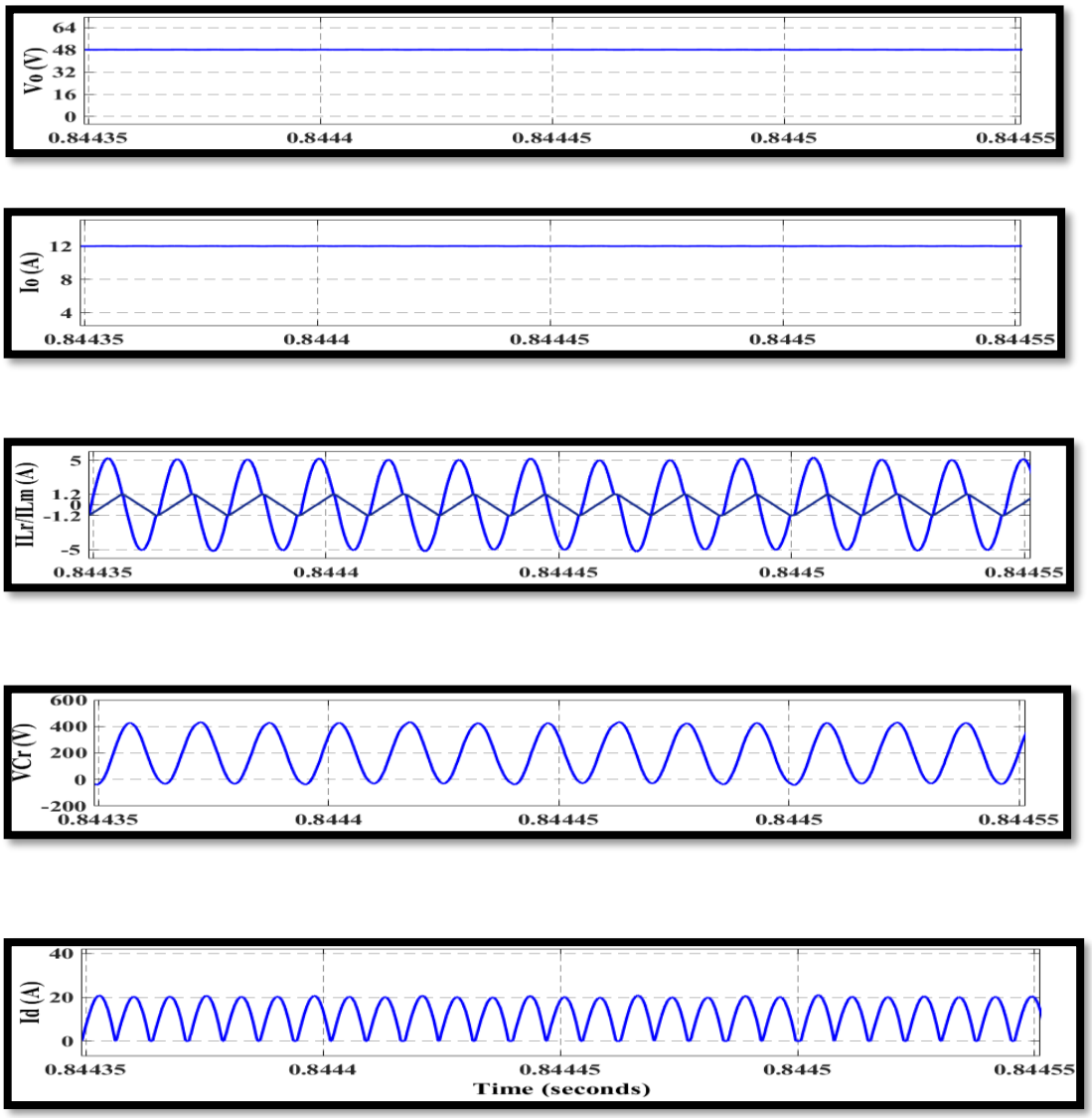

Fig.4.3: Resonant capacitor voltage (VCr), magnetising current (ILm), resonant current (ILr), battery voltage (Vo), battery current (Io), & rectifier current (Id) steady-state performance at load of 576W.

4.4.3 Dynamic Behaviour of PFC-Boost Converter

Fig.4.4 displays dynamic performance of PFC-Boost converter over a variety of input voltages.

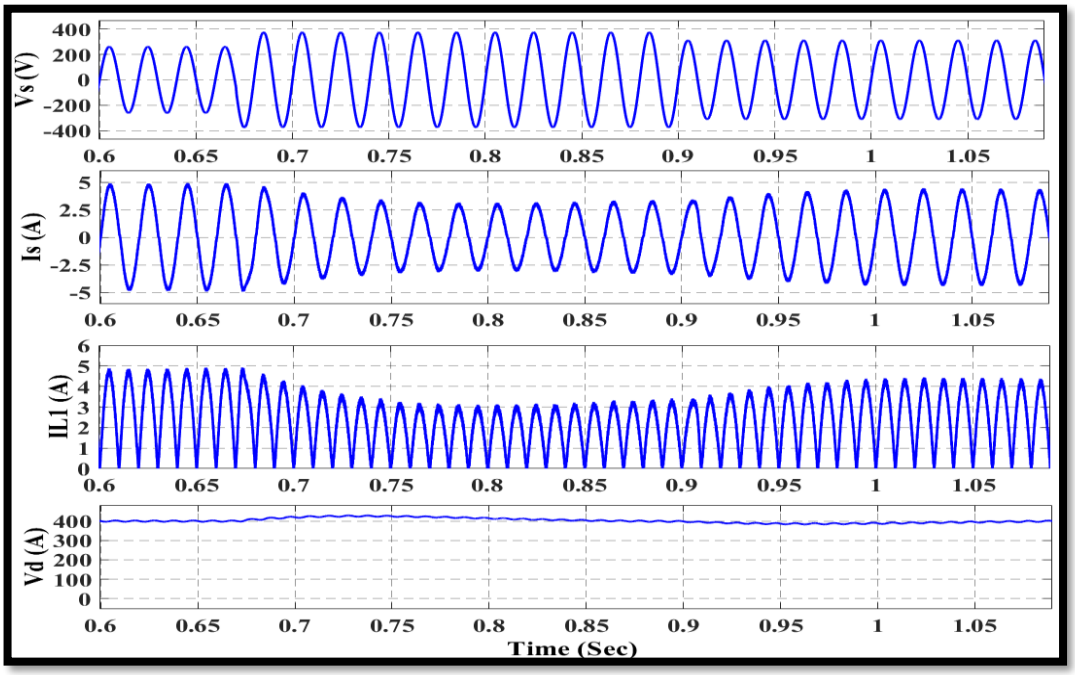

Fig.4.4: The dynamic performance of DC-link voltage (Vdc), input inductor current (IL1) & supply current (Is) at various supply voltages

To examine the dynamic behaviour, PFC-Boost is analysed with different supply voltages ranging from 185V - 265V.In the beginning, V_s was kept at 185V, after that rises up to 265V at 0.655 second and then dropped to 220V at time 0.9 second. Figure 3 shows that the source current decreases as the supply voltage rises and rises as the supply voltage falls with a harmonic free waveform.IL1 is in CCM and the maximum current tread on the heels of AC mains supply maximum current. Vdc is dependent on the V_s and decreases as it drops, but it stabilizes at 400V because the PI-controller maintains good regulation.

4.4.4 LLC Resonant Converter's Dynamic Performance

The second stage converter's dynamic performance is confirmed by changing load from Po = 576W to Po = 720W.PI-Controller well regulates and keeps the output voltage constant. Io goes from 12A to 15A in terms of load current. Figure 4.5 illustrates how the resonant current increases with increasing load while the

magnetising current ILm remains constant at 1.2A. It_i also shows that the LLC resonant current works best when it is near its resonant frequency, which is the ideal operating range. Initially, VCr was 400V, but it had risen as the load raised. The maximum amplitude of Id increase from 20 A to 30 A.

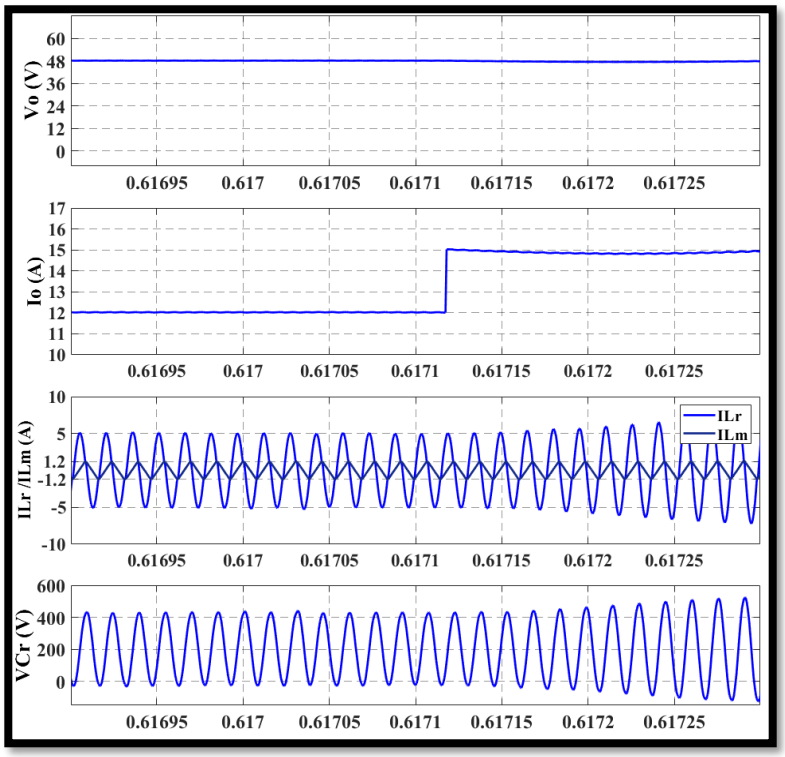

Fig.4.5: Battery voltage (Vo), battery current (Io), resonant current (ILr), magnetising current (ILm), resonant capacitor voltage (VCr), and rectifier current (ID) dynamic performance under different loads.

4.4.5 Changes in Power Factor at Various Input Voltages

The suggested charger is examined with different AC mains supply voltages ranges from 160V to 260V, the maximum THD is measured at 3.06% at higher input voltage of 260V withPF = 0.99952 for the load Po = 576Watt. Table 4.5 summarises all of the information for various V_s and the resulting PFs, I_s, and THD at 576 Watts load.

Table 4.5: Power Factors with respect to Supply Voltage

V_s (volt)	I_s (amp)	Power Factor	THD (%)
160	4.128	0.99961	2.74
170	3.876	0.99965	2.60
180	3.642	0.99968	2.47
190	3.440	0.99968	2.48
200	3.259	0.99970	2.38
210	3.096	0.99965	2.59
220	2.948	0.99967	2.51
230	2.814	0.99964	2.62
240	2.692	0.99963	2.69
250	2.580	0.99957	2.88
260	2.476	0.99952	3.06

4.5 Conclusion

Power factor corrected resonant converter from Half-Bridge LLC is intended for use in electric car battery charging applications.The input current is kept sinusoidal with the help of an APFC boost converter. The proposed topology's steady-state and dynamic performance has been examined with regard to load variation and supply voltage variation. Various input voltages have been used to measure the power factor. With a smooth sinusoidal input current, a good performance has been seen.

CHAPTER 5
A SEPIC PFC FED LLC RESONANT CONVERTER

5.1 Introduction

This research proposes PFC-SEPIC fed HBLLC Resonant Converter for a two-on-board wheeler's private charger. The isolated DC-DC converter in the on-board charger's second stage has the responsibility for controlling the o/p voltage & current based on the intended battery outline. Half-bridge topologies are commonly used for intermediate-power levels, whereas DAB (Dual Active Bridge) or full bridge modules are used for developed ratings and bidirectional power circulation[89]. Because of its ability to operate with zero-voltage switching (ZVS) over such a wide output voltage range, the LLC resonant converter is a good choice. However, under CC and CV conditions, the load, DC relation, and battery-charging voltage can significantly impact the turn-off losses in the switching devices[90]–[94]. The operating frequency of the converter increases over the resonance frequency when the battery is low on power, the voltage is lower than the nominal voltage (CC mode), or the converter is lightly equipped. This results in increased MOSFET turn-off losses on the primary and secondary sides, leading to a significant reduction in efficiency. Unlike the PFC boost-derived converter in the first stage, the LLC converter can reduce turn-off losses by decreasing input voltage and drawing back the switching frequency towards the resonant frequency.

Fig.5.1 depicts the envisaged PFC-SEPIC fed HBLLC Resonant Converter arrangement. In CCM mode, the PFC-SEPIC requires both current and voltage circuits. This converter offers enhanced system efficiency for alternating current mains across an expansive output voltage variety. The chosen technique minimizes both the needed magnetic component size and turn-off losses in the second-stage converter's steep-side switching devices. Additionally, the use of SEPIC converter offers capacitive seclusion and eliminates the inrush current problematic, thereby preventing dips in domestic power supply during EV charging.

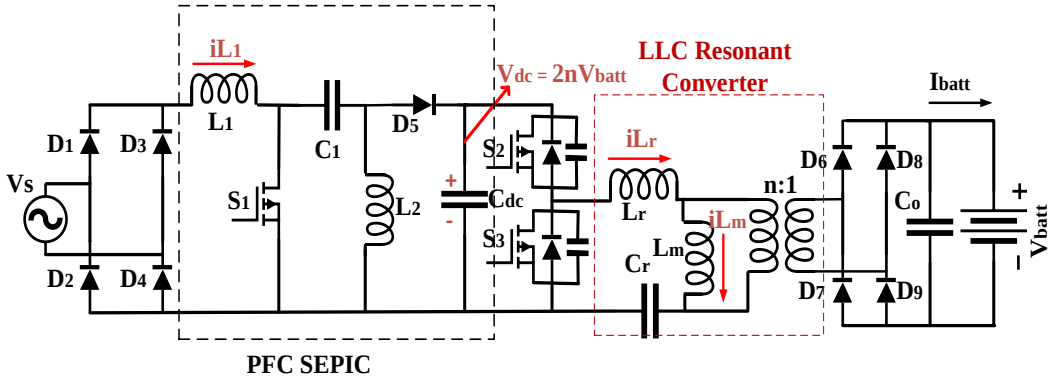

Fig.5.1: Proposed PFC-SEPIC fed HBLLC Resonant Converter

5.2 Design of Proposed Electric Vehicle Battery Charger

The following assumptions are made while designing the parameters for the SEPIC PFC:

1) The devices used here are ideal.
2) Resistor is taken for the battery.

5.2.1 Designing of PFC SEPIC Converter

Specifications for designing the parameters of the PFC SEPIC converter are tabulated in Table 5.1.

Table 5.1: Specifications Considered for SEPIC Converter

Parameters	Variables	Values
Supply Frequency	f_{supply}	50 Hz
Switching Frequency	f_{sw}	50kHz
Supply Voltage	V_s	220V
DC-link Voltage	V_{dc}	300 V
Voltage ripple	ΔV_{dc}	1.5 %
I/P inductor current ripple	ΔI_{Li}	20%
Output Power	P_o	1 kW

Assuming a constant voltage of Vdc for the dc-link, disregarding any fluctuations in voltage ripple across the DC-link capacitor, the duty cycle variation of the SEPIC in a stable condition can be expressed as follows,

$$d(t) = \frac{V_{dc}}{V_{dc}+V_P|\sin(wt)|} \quad (5.1)$$

In which VP represents line voltage's peak value, and angular frequency of the power line is represented by ω, typically set at 100π radians per second.

The duty cycle has the following range,

$$\frac{V_{dc}}{V_{dc}+V_{savg}} \leq d(t) \leq 1 \quad (5.2)$$

The mean value of the input supply voltage, denoted as Vsavg, is determined by the following calculation, assuming a nominal input voltage.

$$V_{savg} = \frac{2\sqrt{2}V_s}{\pi} = \frac{2\sqrt{2}\times 220}{\pi} = 198V \quad (5.3)$$

Putting the values of V_{dc} and V_{savg} in the above eq., duty cycle is found to be 0.6.

The inductance values for L1 and L2 can be computed using the following calculation.

$$L_i = \frac{V_{savg}\times d}{\Delta I_{Li}\times f_{sw}} \quad (5.4)$$

Assuming a current ripple of 20% and a switching frequency of 50 kHz, the inductance values for L1 and L2 are computed to be 2.376 mH.

The capacitance value for the intermediate capacitor denoted as C1, and subject to voltage ripple ΔVC1, is determined using the following calculation.

$$C_1 = \frac{d \times P_o}{\Delta V_{C1} \times V_{dc} \times f_{sw}} \quad (5.5)$$

Assuming fsw of 50kHz and voltage ripple as 20% of Vdc, an output power of 1 kW, a DC-link voltage of 300 V, and a duty cycle of 0.6, the capacitance value for the intermediate capacitor C1 is calculated to be 667 nF.

The capacitance value for CDC (DC-link capacitor), subject to ΔVdc and a supply frequency(fsupply), can be determined using the following calculation.

$$C_{dc} = \frac{P_o}{4\pi \times \Delta V_{dc} \times f_{supply} \times V_{dc}} \quad (5.6)$$

To minimize voltage ripple, a capacitor with a larger value is typically selected. However, this can result in a physically larger capacitor. Therefore, when designing the converter, a trade off b/w ΔVdc and the size of the capacitor must be carefully considered. For example, given a DC-link voltage ripple of 1.5%, the capacitance value for the DC-link capacitor can be calculated to be 1180 μF.

5.2.2 Specifications of HB-LLC Resonant Converter

Table 5.2 tabulates the specifications for determining the component values of a HB-LLC resonant converter.

Table 5.2: Specifications of HB-LLC

Parameters	**Variables**	**Values**
DC-link bus Voltage	V_{DC}	300V
Optimal battery voltage	V_{batt}	57V
Output Power	P_o	1kW
Resonant Frequency	f_r	100kHz

For EV battery charging, the regulated Vdc is supplied to the HB-LLC converter's (turns ratio) of the transformer can be computed using the following equation,

$$n = \frac{V_{dc\_bus}}{2V_{batt}} = \frac{300}{2\times57} = 2.63 \tag{5.7}$$

The resonant current's maximum value, for the converter at the second stage, can be determined using the following calculation,

$$I_{Lr} = \frac{2\pi P_o}{2V_{dc\_bus}} = \frac{2\pi\times1kW}{2\times300} = 10.46\ A \tag{5.8}$$

Assuming a resonance frequency of 100 kHz, the capacitance value for the resonant capacitor can be determined using the following calculation,

$$C_r = \frac{I_{Lr}}{2\pi f_r V_{dc\_bus}/_2} = \frac{10.46}{2\pi\times100\times10^3\times300/_2} \tag{5.9}$$

$$= 111nF$$

Inductance ratio(m) in this project has been chosen as 5. The resonant and magnetizing inductances can be calculated as,

$$L_r = \frac{1}{(2\pi f_r)^2 C_r} = \frac{1}{(2\pi\times100\times10^3)^2\times111n} = 22.8\mu H \tag{5.10}$$

$$L_m = m \times L_r = 5 \times 22.8\mu H = 114\mu H \tag{5.11}$$

5.3 Control Techniques of Proposed Charger

In this work, a two-loop structure of APFC is utilized to improve the power factor. The outer loop controls the DC-link voltage through a voltage control loop. The reference DC-link voltage is generated by measuring the battery voltage, $V_{dc} = 2nV_{batt}$, and continuously adjusting the DC-link voltage accordingly. The difference b/w the measured DC-link voltage and the reference DC-link voltage, leads to an error voltage, which is subsequently manipulated using a proportional-integral (PI) controller, in order to produce a modulating current signal. After that the product of this signal and the unit prototype of the AC mains voltage creates the base current for the primary inductor. The PWM gate pulses for the switch in the SEPIC is generated by utilizing the primary inductor current feedback. Following this, the resulting current is compared to the base current, generating a current error signal that is processed using a PI-based current controller.

Furthermore, the secondary stage of the system employs LLC converter, which receives the Vdc and uses a PI voltage controller to regulate the output voltage. The pulses for the switches of the HB-LLC converter are created by the resulting rate signal which is administered by the PFM controller. Fig.5.2 depicts the control technique used in this two stage EV battery charger.

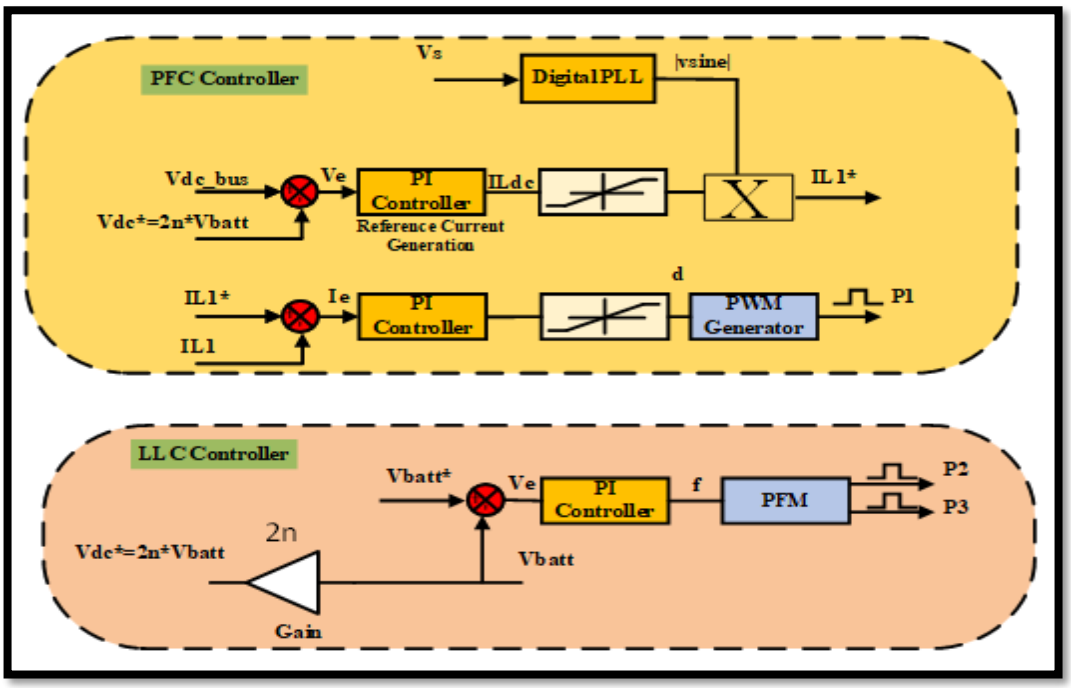

Fig.5.2: Control technique of the proposed charger

5.4 Simulation Result and Discussion

In order to verify the proposed converter, simulations were conducted using MATLAB/Simulink software. The simulations covered battery voltages for a broader range and different Vs values for various loads. Table 5.3 summarizes all the parameters calculated in Section 5.2.

Table 5.3: Parameters of The Proposed Charger

Parameters	**Variables**	**Values**
Supply Frequency	f_{supply}	50 Hz
Switching Frequency	f_{sw}	50kHz
Supply Voltage	V_s	220V
Output Power	P_o	1 kW
DC-link Capacitor	C_{dc}	1180 μF
Resonant frequency	f_r	100kHz
Primary & Secondary Inductors	L_1 & L2	2.376mH
Resonant Inductor	L_r	22.8 μH
DC-link Voltage	V_{dc}	300 V
Resonant Capacitor	C_r	111 nF
Magnetizing inductor	L_m	*114 μH*

5.4.1 Validation of the Broad Voltage (V_{batt}) range and the DC-link Voltage (V_{dc})

The simulations were performed over a range of Vbatt and Vs for various loads. The Vdc is designed to track the Vbatt, which is expressed by V*dc = 2nVbatt. The simulation results indicate that at Vbatt = 80V, the Vdc-bus = 419V, while at Vbatt = 48V, the Vdc-bus = 250V. This is shown in Fig.5.3.

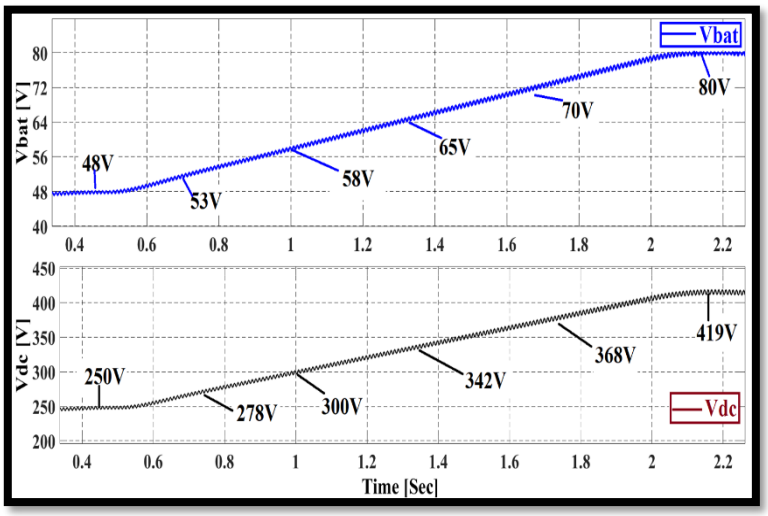

Fig.5.3: Variance of DC-link bus voltage in comparison to battery voltage

5.4.2 Testing the EV Charger at Several Supply Voltages

Simulations were conducted for various Vs values ranging from (85-220) Vrms, with a Vbatt of 57V & Po = 1kW. The Is (source current) demonstrated admirable performance across the whole assortment of Vs, exhibiting THD value less than 3% and unity PF. Notably, the Vbatt was unaffected by the change in Vs, as demonstrated in Fig.5.4.

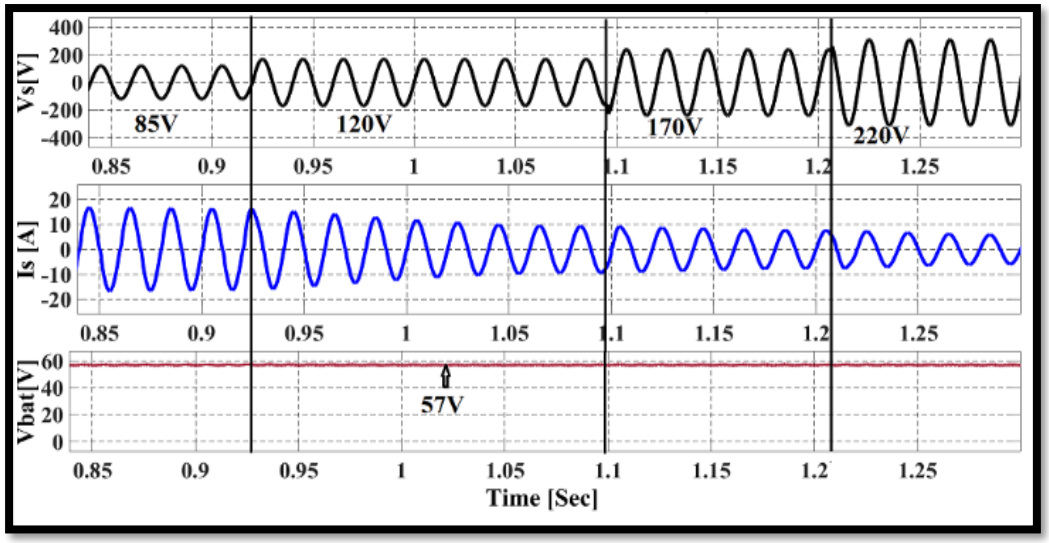

Fig.5.4: Simulink results of battery voltage (V_{bat}), source current (I_s) under different supply voltages (V_s)

5.4.3 Testing the EV Charger at Different Loads

Furthermore, simulations were run for various loads which extends from 1kW-100W, with the V_{batt} kept fixed at 57V and by contrasting the battery current the load is varied. The peak current achieved was 17.54A at 1kW load, while the least value of current observed was 1.57A at a light load of 100W. Little bit more ripple was ascertained in the battery voltage & current at high loads in comparison to the light loads. Fig.5.5 depicts the effectiveness.

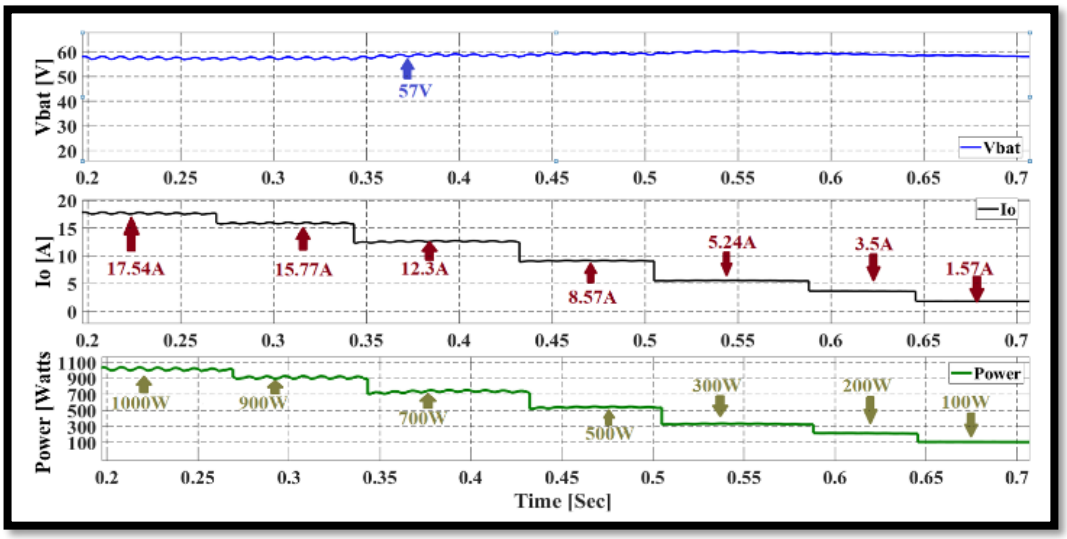

Fig.5.5: EV battery charger's Performance at different loads.

5.4.4 At Nominal Supply Voltage (V_s) and Nominal Battery Voltage (V_{batt})EV Battery Charger's Performance

The working of the system at power 700W & source voltage 220V is demonstrated in Fig.5.6. It's shown that the source voltage (Vs)is followed by the i/p current with upf. For a Vbatt of 57V the Vdc reaches to 300V. The 1o inductor and 2o current are in CCM. With a peak amplitude of 370V, Fig.5.6 shows the waveform of the intermediate capacitance. The FFT analysis with TDD of 1.61% is shown in Fig.5.7.

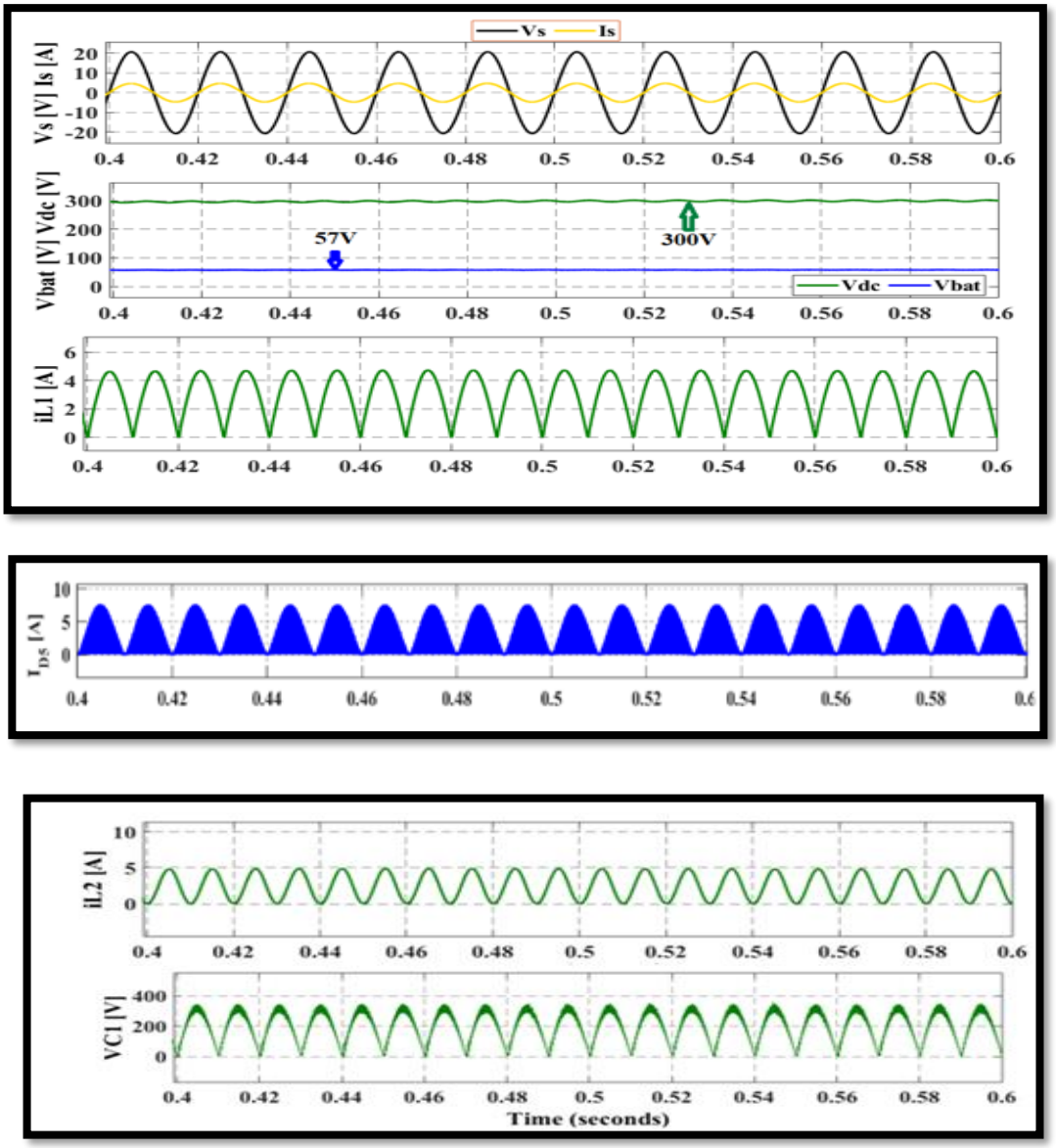

Fig.5.6: Essential output waveform depicting I_s, V_{dc}, V_{batt}, iL_1, I_{DS}, iL_2, V_{C1} at V_s =220V & P_0 = 700 W.

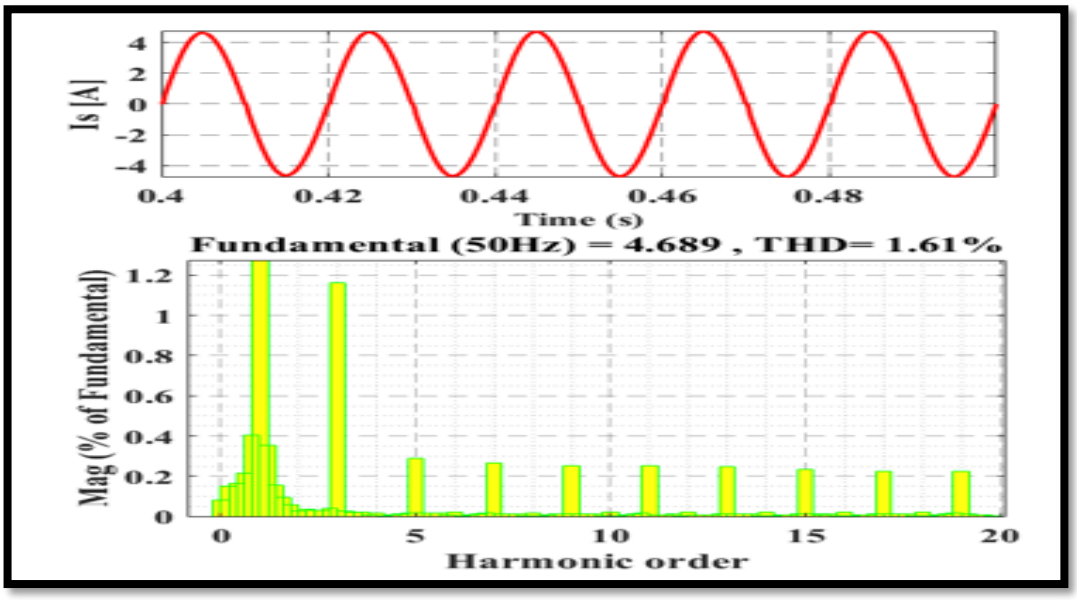

Fig.5.7: At P_o=700W & V_{batt} = 57V, the FFT Analysis of I_S (Source Current)

Fig.5.8 shows the working of HB-LLC resonant converter. The HB-LLC converter is performing near resonantt frequency (f_r), this is shown by the current waveforms of magnetizing & resonant inductors. The maximum value of the voltage V_{Cr} is 400V. The zero-voltage switching (ZVS)is shown by the current & voltage waveforms of MOSFET switch.

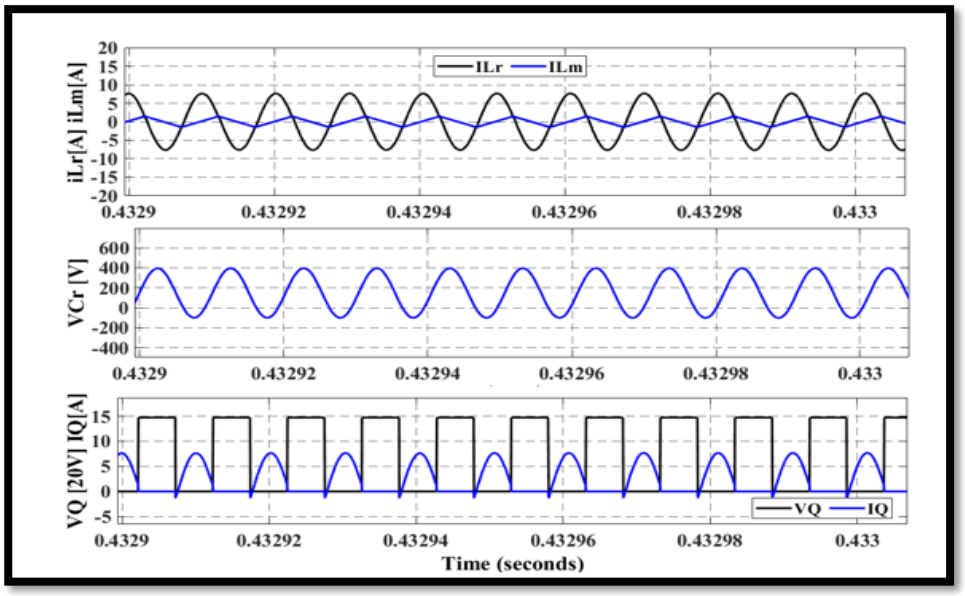

Fig.5.8: The essential output waveform of iLr, iLm, VCr, throughout the MOSFET switch at Po = 700W & Vs = 220V are shown.

5.4.5 The EV Battery Charger's Overall Performance

The proposed approach exhibits superior efficiencies at different load levels when compared to the conventional method, which maintains a constant DC-link and wide frequency variation for varying loads. Overall performance at different supply voltages (Vs), loads and battery voltages (Vbatt)are tabulated in Table 5.4.

Table 5.4: Overall Performance of The On-Board Charger

RMS value of Vs (Volts)	**Is (Amp)**	**Vdc (Volts)**	**Po (Watt)**	**Vbatt (Volts)**	**Io (Amp)**	**% TDD**
220	9.34	419	1970	80	24.63	2.547
220	6.23	342	1300	65	19.89	1.873
220	4.77	300	1000	58	17.54	1.453
170	6.25	300	1000	58	17.54	2.456
85	12.4	300	1000	58	17.54	3.895
220	3.35	300	700	58	12.30	1.612
220	1.43	300	300	58	5.24	2.135
220	0.5	300	100	58	1.57	2.656

5.5 Conclusion

A power factor correction mechanism has been developed utilizing a SEPIC, which is preceded by an HB-LLC resonant converter. For the entire battery voltage (Vbatt) range of 48-80V, the second stage converter operates adjacent to the fr (resonance frequency). The conceptual layout has been validated via simulation across different input voltages (Vs) ranging from 85Vrms to 220Vrms, as well as varying battery voltages of 58V-70V under various load conditions. The total harmonic distortion (TDD) is less than 3.895% for an input voltage of 85V. The proposed approach yields a cumulative efficiency of 95% at a load of 1kW and 89% at lighter loads, which is significantly better than traditional techniques.

CHAPTER 6
CONCLUSIONS AND FUTURE SCOPE

6.1 Conclusion

Electric vehicles are widely used in the modern world. One of the most crucial components of electric vehicles is the battery. The only reason an electric vehicle (EV) is superior to a car with a petrol or diesel engine is because its battery performs better, and charging a battery is an essential component. So, various EV battery chargers with various charging topologies are being implemented. On-board electric vehicle charger is among one of those topologies which has been implemented here in this thesis on MATLAB.

Two stage chargers have been adopted here, in which the first stage is the PFC converter and the Half Bridge LLC resonant converter forms the second stage. Two different converters have been used as the first stage and experimented separately. First, PFC Boost converter has been taken as the first stage and later on the effect with PFC SEPIC has been observed by using it at the first stage. It has also been observed that the LLC resonant converter works at its best around the resonance frequency.

Power factor corrected resonant converter from Half-Bridge LLC is intended for use in electric car battery charging applications. The input current is kept sinusoidal with the help of an APFC boost converter. The proposed topology's steady-state and dynamic performance has been examined with regard to load variation and supply voltage variation. Various input voltages have been used to measure the power factor. It has also been observed that the quality of power of AC mains supply current improves with a maximum THD of 3.06 % as illustrated in chapter 4. With a smooth sinusoidal input current, a good performance has been seen. At the same time one more conclusion was made that this configuration goes through a large inrush current from input side for a period of 8.35 msec.

To remove the large inrush current discussed in above configuration a SEPIC fed HB-LLC resonant converter has been adopted and observed. The inrush current is suppressed by the intermediate capacitor present in SEPIC, as discussed in chapter 5. For the entire battery voltage (Vbatt) range of 48-80V, the second stage converter operates adjacent to the fr (resonance frequency) for the improved performance. The

conceptual layout has been validated via simulation across different input voltages (Vs) ranging from 85Vrms to 220Vrms, as well as varying battery voltages of 58V-70V under various load conditions. The total harmonic distortion (TDD) is less than 3.895% for an input voltage of 85V. The proposed approach yields a cumulative efficiency of 95% at a load of 1kW and 89% at lighter loads, which is significantly better than traditional techniques.

5.2 Future Scope

The two-stage topology can further be tested using PFC Cuk converter as the first stage and its effect will be observed and also compared with the previous two PFC configurations. Furthermore, hardware implementation of the on-board charger configuration can be done in future for commercializing the prototype model discussed in this thesis.

REFERENCES

[1] D. L. Anderson, "An Evaluation of Current and Future Costs for Lithium-ion Batteries for Use in Electrified Vehicle Powertrains," Duke University, 2009.

[2] A. Y. Saber and G. K. Venayagamoorthy, "One Million Plug-in Electric Vehicles on the Road by 2015," in *2009 12th International IEEE Conference on Intelligent Transportation Systems*, 2009, pp. 1–7.

[3] M. Yilmaz and P. T. Krein, "Review of Battery Charger Topologies, Charging Power Levels and Infrastructure for Plug-in Electric and Hybrid Vehicles," *IEEE Trans. Power Electron.*, vol. 28, no. 5, pp. 2151–2169, May 2012.

[4] S. Dusmez, A. Cook, and A. Khaligh, "Comprehensive Analysis of High Quality Power Converters for Level 3 off-board Chargers," in *2011 IEEEVehicle Power and Propulsion Conference*, 2011, pp. 1–10.

[5] L. K. Cowan, "5.2 million Strong: Report Predicts 46x Increase in EV Sales by 2017." [Online]. Available: http://inhabitat.com/5-2-million-strong-report-

[6] Texas Instruments, "Hybrid and Electric Vehicle Solutions Guide", http://www.ti.com/lit/ml/szza058a/szza058a.pdf

[7] K. T. Chau and Y. S. Wong, "Overview of power management in hybrid electric vehicles", Energy Conversion and Management, vol. 43, Issue 15, pp. 1953-1968, 2002.

[8] L. Siguang, Z. Chengning, and X. Shaobo, "Research on Fast Charge Method for Lead-acid Electric Vehicle Batteries", in Proc. IEEE ISA'09, May 2009, pp. 1-5.

[9] Richard Redl, "Batteries for Beginners" in Proc. APEC, Feb.5-9, 2012, pp.

[10] A. S. J1772, "ASE Electric Vehicle and Plug-in Hybrid Electric

Vehicle Conductive Charge Coupler," 2011.

[11] K. Morrow, D. Karner, and J. Francfort, "Plug-in Hybrid Electric Vehicle Charging Infrastructure Review," in US Department of Energy-Vehicle Technologies Program, 2008.

[12] L. De Sousa, B. Silvestre, and B. Bouchez, "A Combined Multiphase Electric Drive and Fast Battery Charger for Electric Vehicles," in 2010 IEEE Vehicle Power and Propulsion Conference, 2010, pp. 1–6.

[13] D. P. Tuttle and R. Baldick, "The Evolution of Plug-In Electric Vehicle-Grid Interactions," IEEE Trans. Smart Grid, vol. 3, no. 1, pp. 500–505, Mar. 2012.

[14] K. Bullis, "Forget Battery Swapping: Tesla Aims to Charge Electric Cars in Five Minutes," MIT Technology Review, 2013.[Online].Available:http://www.technologyreview.com/news/516876/forget-battery-swapping- tesla-aims-to-charge-electric-cars-in-five-minutes/. [Accessed: 19-Jul-2013].

[15] C. Costa, "Tesla Supercharging Stations will Soon Charge EVs in 5-minutes,"GadgetReview,2013.[Online].Available:http://www.gadgetreview.com/2013/07/tesla-supercharging-stations-will-soon-charge-evs-in-5-minutes.html. [Accessed: 19-Jul-2013].

[16] S. W. Hadley and A. A. Tsvetkova, "Potential Impacts of Plug-in Hybrid Electric Vehicles on Regional Power Generation," Electr. J., vol. 22, no. 10, pp. 56–68, Dec. 2009.

[17] S. Campbel and E. Hoffman, "Eletrification of the Transportation System," in Initiative, MIT Energy, 2010.

[18] I. C. Commission, "Initiative on Plug-in Electric Vehicles, Commonwealth Edison Company, Initial Assessment of the Impact of the Introduction of Plug- in Electric Vehicles on the Distribution

System," 2010.

[19] M. Etezadi-Amoli, K. Choma, and J. Stefani, "Rapid-Charge Electric-Vehicle Stations," IEEE Trans. Power Deliv., vol. 25, no. 3, pp. 1883–1887, Jul. 2010.

[20] J. C. Gomez and M. M. Morcos, "Impact of EV Battery Chargers on the Power Quality of Distribution Systems," IEEE Trans. Power Deliv., vol. 18, no. 3, pp. 975–981, Jul. 2003.

[21] T. Anegawa, "Desirable Characteristics of Public Quick Charger," in PHEV 09 Montreal, 2009.

[22] T. Anegawa, "Development of Quick Charging System for Electric Vehicle," in Tokyo Electric Power Company, 2010.

[23] D. Aggeler, F. Canales, H. Zelaya, D. La Parra, A. Coccia, N. Butcher, and O. Apeldoorn, "Ultra-fast DC-charge Infrastructures for EV-mobility and Future Smart Grids," in IEEE PES Innovative Smart Grid Technologies Conference Europe, 2010, pp. 1–8.

[24] C. Isidore, "Tesla Unveils 90-second Battery-pack Swap," CNN Money,2013.[Online].Available:http://money.cnn.com/2013/06/21/ autos/tesla-battery- swap/index.html. [Accessed: 19-Jul-2013].

[25] H.-Y. Mak, Y. Rong, and Z.-J. M. Shen, "Infrastructure Planning for Electric Vehicles with Battery Swapping," SSRN Electron. J., Mar. 2012.

[26] W.-Q. Tian, J.-H. He, J.-C. Jiang, L.-Y. Niu, and X.-J. Wang, "Research on Dispatching Strategy for Coordinated Charging of Electric Vehicle Battery Swapping Station," Power Syst. Prot. Control, vol. 40, no. 21, pp. 114–119, 2012.

[27] S. Bai, D. Yu, and S. Lukic, "Optimum Design of an EV/PHEV Charging Station with DC Bus and Storage System," in 2010 IEEE

Energy Conversion Congress and Exposition, 2010, pp. 1178–1184.

[28] C. Lin, C. Hsieh, K. Chen, Chia-Hsiang Lin, Chun-Yu Hsieh, and Ke-Horng Chen, "A Li-Ion Battery Charger with Smooth Control Circuit and Built-In Resistance Compensator for Achieving Stable and Fast Charging," IEEE Trans. Circuits Syst. Regul. Pap., vol. 57, no. 2, pp. 506–517, Feb. 2010.

[29] S. Li, C. Zhang, and S. Xie, "Research on Fast Charge Method for Lead-Acid Electric Vehicle Batteries," in 2009 International Workshop on Intelligent Systems and Applications, 2009, pp. 1–5.

[30] Liang-Rui Chen, Roy-Chaoming Hsu, Chuan-Sheng Liu, Wei-Zhan Yen, Neng-Yi Chu, and Yuan-Li Lin, "A Variable Frequency Pulse Charge Strategy for Li-ion Battery," in IEEE International Symposium on Industrial Electronics, 2005, vol. 3, pp. 995–1000.

[31] A. Khaligh and S. Dusmez, "Comprehensive Topological Analysis of Conductive and Inductive Charging Solutions for Plug-In Electric Vehicles," IEEE Trans. Veh. Technol., vol. 61, no. 8, pp. 3475–3489, Oct. 2012.

[32] A. Khaligh and L. Zhihao, "Battery, Ultracapacitor, Fuel Cell, and Hybrid Energy Storage Systems for Electric, Hybrid Electric, Fuel Cell, and Plug-In Hybrid Electric Vehicles: State of the Art," IEEE Trans. Veh. Technol., vol. 59, no. 6, pp. 2806–2814, Jul. 2010.

[33] X. Zhang, C. Li, C. Yao, L. Fu, F. Guo, and J. Wang, "An Isolated DC/DC Converter with Reduced Number of Switches and Voltage Stresses for Electric and Hybrid Electric Vehicles," in IEEE Applied Power Electronics Conference and Exposition, 2013.

[34] "Car Prototype Generates Electricity, And Cash," Science Daily, 2007.[Online].Available:http://www.sciencedaily.com/releases/2007/12/071203133532.htm. [Accessed: 21-Jul-2013].

[35] H. Lund and W. Kempton, “Integration of Renewable Energy into the Transport and Electricity Sectors through V2G,” Energy Policy, vol. 36, no. 9, pp. 3578–3587, Sep. 2008.

[36] C. Guille and G. Gross, “A Conceptual Framework for the Vehicle-to-grid (V2G) Implementation,” Energy Policy, vol. 37, no. 11, pp. 4379–4390, Nov. 2009.

[37] M.C. Kisacikoglu, B. Ozpineci, L.M. Tolbert, “Reactive power operation analysis of a single-phase EV/PHEV bidirectional battery charger,” Power Electronics and ECCE Asia (ICPE & ECCE), 2011 IEEE 8th International Conference on, vol., no., pp.585-592, May 30 2011-June 3 2011

[38] G. Glanzer, T. Sivaraman, J.I. Buffalo, M. Kohl, H. Berger, "Cost-efficient integration of electric vehicles with the power grid by means of smart charging strategies and integrated on-board chargers," Environment and Electrical Engineering (EEEIC), 2011 10th International Conference on, vol., no., pp.1-4, 8- 11 May 2011

[39] C.B. Toepfer, “Charge! EVs power up for the long haul,” Spectrum, IEEE, vol.35, no.11, pp.41-47, Nov 1998

[40] Erb, D.C.; Onar, O.C.; Khaligh, A.; "Bi-directional charging topologies for plug-in hybrid electric vehicles," Applied Power Electronics Conference and Exposition (APEC), 2010 Twenty-Fifth Annual IEEE, vol., no., pp.2066-2072, 21-25 Feb. 2010

[41] Jim Francfort, “Electric Vehicle Charging Levels and Requirements Overview”, Clean Cities December 2010 Webinar, http://www1.eere.energy.gov

[42] Ingram, “Charging your electric car at home: What you need to know”, Venture Beat, August 13, 2010.

[43] Nissan;“ChargingFAQ”,[online].Available:http://www.nissanusa.co

m/leaf-electriccar/faq/list/charging#/leafelectriccar/faq/list/charging

[44] NEC Corporation of America, “Portland General Electric Opens North America’s First Public-Use Quick-Charge Station,” Portland, OR, August 5, 2010.

[45] SAE International, “Ground Vehicle Standards Newsletter”,vol. 1, issue 3, October 2010.

[46] X. Navarro, “The European standard charging plug for cars is selected after Mennekes design” Autoblog, May 20, 2009.

[47] CHAdeMO,“What is CHAdeMO?” [Online]. Available: http://chademo.com/01_What_is_CHAdeMO.html

[48] R.Surada, and A. Khaligh, "A novel approach towards integration of propulsion machine inverter with energy storage charger in plug-in hybrid electric vehicles," in Proc.IECON’10, Nov. 7-10, 2010, pp. 2493-2498.

[49] D. Erickson, R.W. and Maksimovic, Fundamentals of Power Electronics. Springer, 2001

[50] Chan, C.C. and Chau, K.T., "An overview of power electronics in electric vehicles," IEEE Trans. on Industrial Electronics, Volume 44, Issue 1, February 1997, Page(s): 3 – 13.

[51] J. G. Hayes, "Battery Charging Systems for Electric Vehicles," Electric Vehicles - A Technology Roadmap for the Future," Digest No. 1998/262, IEE Colloquium on page(s): 4/1-4/8, May 1998.

[52] I.A. Khan, "Battery chargers for electric and hybrid vehicles," Power Electronics in Transportation, Proceedings, 20-21 Oct. 1994, Page(s): 103-112.

[53] Gyu-YeongChoe; Jong-Soo Kim; Byoung-Kuk Lee; Chung-Yuen Won; Tea-Won Lee; , "A Bi-directional battery charger for electric

vehicles using photovoltaic PCS systems," Vehicle Power and Propulsion Conference (VPPC), 2010 IEEE , vol., no., pp.1-6, 1-3 Sept. 2010

[54] R. Severns, “Topologies for Three Elements Resonant Converters,” in IEEE APEC Rec., 1990, pp. 712-722.

[55] R. Oruganti and F.C. Lee, “Resonant Power Processors, Part 2: Methods of Control,” IEEE Trans. on Industrial Application, 1985.

[56] R. Severns, “Topologies for Three Element Resonant Converters,” Proc. IEEE APEC ’90, 1990, pp. 712-722.

[57] VatcheVorperian, Analysis of Resonant Converters, Dissertation, California Institute of Technology, 1984.

[58] R. Farrington, M.M. Jovanovic, and F.C. Lee, “Analysis of Reactive Power in Resonant Converters,” Proc. IEEE PESC ’92, 1992.

[59] P. Calderira, R. Liu, D. Dalal, W.J. Gu, “Comparison of EMI Performance of PWM and Resonant Power Converters,” Proc. IEEE PESC ’93, 1993, pp. 134-140.

[60] T. Higashi, H. Tsuruta, M. Nakahara, “Comparison of Noise Characteristics for Resonant and PWM Flyback Converters,” Proc. IEEE PESC ’98, 1998, pp. 689-695.

[61] K.H. Liu, “Resonant Switches Topologies and Characteristics,” Proc. IEEE PESC’85, 1985, pp. 106-116.

[62] J. O. Groves and F. C. Lee, “Small Signal Analysis of Systems with Periodic Operating Trajectories,” Proc. VPEC Annual Seminar, 1988, pp. 224-235.

[63] J. O. Groves, “Small-Signal Analysis Using Harmonic Balance Methods,” Proc. IEEE PESC, 1991, pp. 74–79.

[64] E. X. Yang, “Extended Describing Function Method for Small-Signal Modeling of Switching Power Circuit,” Proc. VPEC Annual Seminar, 1994, pp.87-96.

[65] E. X. Yang, F. C. Lee and M. Jovanovic, “Small-Signal Modeling of Series and Parallel Resonant Converters,” Proc. IEEE APEC, 1992, pp. 785-792.

[66] Eric X. Yang,Extended Describing Function Method for Small-Signal Modeling of Resonant and Multi-Resonant Converters, Dissertation, Virginia Tech, Blacksburg, VA, February 1994.

[67] R.C. Wong and J. O. Groves, “An Automated Small-Signal Frequency- Domain Analyzer for General Periodic-Operating Systems as Obtained via Time-Domain Simulation,” Proc. IEEE PESC, 1995, pp. 801-808.

[68] R. Oruganti, J. Yang, and F.C. Lee, “State Plane Analysis of Parallel Resonant Converters,” Proc. IEEE PESC ’85, 1985.

[69] R. Liu, I. Batarseh, C.Q. Lee, “Comparison of Capacitively and Inductively Coupled Parallel Resonant Converters,” IEEE Trans. on Power Electronics, 1993, pp. 445- 454, vol.8, issue 4.

[70] M. Emsermann, “An Approximate Steady State and Small Signal Analysis of the Parallel Resonant Converter Running Above Resonance,” Proc. Power Electronics and Variable Speed Drives ’91, 1991, pp. 9-14.

[71] Y.G. Kang, A.K. Upadhyay, D. Stephens, “Analysis and Design of a Half Bridge Parallel Resonant Converter Operating Above Resonance,” Proc. IEEE IAS ’98, 1998, pp. 827-836.

[72] Robert L. Steigerwald, “A Comparison of Half Bridge Resonant Converter Topologies,” IEEE Trans. on Power Electronics, 1988, pp. 174-182.

[73] M. Zaki, A. Bonsall, I. Batarseh, “Performance Characteristics for the Series Parallel Resonant Converter,” Proc. Southcon ’94, 1994, pp.573-577.

[74] A.K.S. Bhat, “Analysis, Optimization and Design of a Series Parallel Resonant Converter,” Proc. IEEE APEC ’90, 1990, pp. 155-164.

[75] Fairchild Semiconductor Corporation, “Application Note AN-4151: Half Bridge LLC Resonant Converter Design Using FSFR-series Fairchild Power Switch” Rev1.0.0, 10/09/2007

[76] STMicroelectronics, “Application Note AN-2450: LLC resonant half-bridge converter design guideline”, Rev5, 10/2007

[77] Microchip Technology Inc. “AN1336: DC/DC LLC Reference Design Using the dsPIC® DSC”, 2010

[78] A. Khaligh, and S. Dusmez, "Comprehensive topological analysis of conductive and inductive charging solutions for plug-in electric vehicles," IEEE Trans. Veh. Technol., vol. 61, no. 8, pp. 3475-3489, Oct. 2012.

[79] C.-Y. Oh, D.-H. Kim, D.-G. Woo, W.-Y. Sung, Y.-S. Kim, and B.-K. Lee, “A High-Efficient Nonisolated Single-Stage On-board Battery Charger for Electric Vehicles,” IEEE Trans. Power Electron., vol. 28, no. 12, pp. 5746–5757, Dec. 2013.

[80] H.-S. Kim, M.-H. Ryu, J.-W. Baek, and J.-H. Jung, “High-Efficiency Isolated Bidirectional AC–DC Converter for a DC Distribution System,” IEEE Trans. Power Electron., vol. 28, no. 4, pp. 1642–1654, Apr. 2013

[81] F. Musavi, M. Craciun, D. S. Gautam, W. Eberle, and W. G. Dunford, “An LLC Resonant DC–DC Converter for Wide Output Voltage Range Battery Charging Applications,” IEEE Trans. Power Electron., vol. 28, no. 12, pp. 5437–5445, Dec. 2013

[82] B. Gu, C.-Y. Lin, B. Chen, J. Dominic, and J.-S. Lai, “Zero Voltage-Switching PWM Resonant Full-Bridge Converter with Minimized Circulating Losses and Minimal Voltage Stresses of Bridge Rectifiers for Electric Vehicle Battery Chargers,” IEEE Trans. Power Electron., vol. 28, no. 10, pp. 4657–4667, Oct. 2013.

[83] H. Wang and F. Blaabjerg, “Reliability of Capacitors for DC-Link Applications in Power Electronic Converters—An Overview,” IEEE Trans. Ind. Appl., vol. 50, no. 5, pp. 3569–3578, Sep. 2014.

[84] G. Pledl, M. Tauer, and D. Buecherl, “Theory of operation, design procedure and simulation of a bidirectional LLC resonant converter for vehicular applications,” in IEEE Vehicle Power and Propulsion Conference (VPPC), 2010, pp. 1-5.

[85] G. Pledl, M. Tauer, and D. Buecherl, “Theory of operation, design procedure and simulation of a bidirectional LLC resonant converter for vehicular applications,” in IEEE Vehicle Power and Propulsion Conference (VPPC), 2010, pp. 1-5.

[86] Hong Huang, “Designing an LLC Resonant Half-Bridge Power Converter,” Texas Instruments (TI) Power Supply Design Seminar, SEM1900, 2010, TI Literature No. SLUP263

[87] R. Beiranvand, B. Rashidian, M. R. Zolghadri, and S. M. H. Alavi, “Using LLC Resonant Converter for Designing Wide-Range Voltage Source,” IEEE Trans. Ind. Electron., vol. 58, no. 5, pp. 1746–1756, 2011.

[88] Hong Huang, “Designing an LLC Resonant Half-Bridge Power Converter,” Texas Instruments (TI) Power Supply Design Seminar, SEM1900, 2010, TI Literature No. SLUP263.

[89] S. Alatai, M. Salem, I. Alhamrouni, D. Ishak, A. Bughneda, and M. Kamarol, “Design Methodology and Analysis of Five-Level LLC Resonant Converter for Battery Chargers,” Sustain., vol. 14, no. 14,

2022, doi: 10.3390/su14148255.

[90] S. Ketsingsoi and Y. Kumsuwan, “An off-line battery charger based on buck-boost power factor correction converter for plug-in electric vehicles,” Energy Procedia, vol. 56, no. C, pp. 659–666, 2014, doi: 10.1016/j.egypro.2014.07.205.

[91] T. N. Gücin, M. Biberoğlu, and B. Fincan, “Constant frequency operation of parallel resonant converter for constant-current constant-voltage battery charger applications,” J. Mod. Power Syst. Clean Energy, vol. 7, no. 1, pp. 186–199, 2019, doi: 10.1007/s40565-018-0403-7.

[92] Y. Wang, O. Lucia, Z. Zhang, S. Gao, Y. Guan, and D. Xu, “A review of high frequency power converters and related technologies,” IEEE Open J. Ind. Electron. Soc., vol. 1, no. August, pp. 247–260, 2020, doi: 10.1109/OJIES.2020.3023691.

[93] R. Beiranvand, B. Rashidian, M. R. Zolghadri, and S. M. H. Alavi, “A design procedure for optimizing the LLC resonant converter as a wide output range voltage source,” IEEE Trans. Power Electron., vol. 27, no. 8, pp. 3749–3763, 2012, doi: 10.1109/TPEL.2012.2187801.

[94] M. A. Elkeiy, Y. N. Abdelaziz, M. S. Hamad, A. S. Abdel-Khalik, and M. Abdelrahem, “Multiport DC-DC Converter with Differential Power Processing for Fast EV Charging Stations,” Sustain., vol. 15, no. 4, 2023, doi: 10.3390/su15043026.

LIST OF PAPERS & CERTIFICATES

[1] Satyamit Kumar, Narendra Kumar, "A Boost PFC fed LLC Resonant Converter for Electric Vehicle Application", *IEEE 7th International Conference on Emerging Trends in Engineering, Science and Technology (ICETEST 2023)*, Thrissur, Kerala, India (19-21 April 2023) **(Presented)**

ICETEST 2023

7TH INTERNATIONAL CONFERENCE ON EMERGING TRENDS IN ENGINEERING, SCIENCE AND TECHNOLOGY
19-21 April 2023

CERTIFICATE

This is to certify that

Mr/Ms/Dr SATYAMIT KUMAR

Delhi Technological University

has presented a paper titled

A Boost PFC fed LLC Resonant Converter for Electric Vehicle Application

in the

International Conference on
Power Instrumentation Control and Computing
PICC 2023

under the aegis of the

7th International Conference on Emerging Trends in Engineering, Science and Technology
ICETEST 2023

"Society, Energy & Environment - Showcasing the Roadmap for Tomorrow"

organised by Govt. Engineering College Thrissur

during 19 - 21 April 2023.

Dr. JAYAN A R
Organising Secretary

Dr. UMA SYAMKUMAR
Organising Secretary

Dr. SATISH K P
Organising Chairman

Funded by :

Technical Education Quality Improvement Programme
TEQIP

Organised by :

Govt. Engineering College
Thrissur - 680009, Kerala
www.gectcr.ac.in

[2] Satyamit Kumar, Narendra Kumar, “A SEPIC PFC fed LLC Resonant Converter for EV Battery Charger Applications”, *IEEE 4th International Conference of Emerging Technology (INCET 2023)*, Belagavi, Karnataka, India (26th to 28th May 2023) **(Presented)**

Jain College of Engineering
Belagavi, India

IEEE BANGALORE SECTION

4th International Conference of Emerging Technology
(INCET 2023)

26th – 28th May 2023

Certificate

This is to certify that Dr./Prof./Mr./Ms. Satyamit Kumar has presented paper entitled A SEPIC PFC fed LLC Resonant converter For EV Battery Charger Applications in 4th International Conference of Emerging Technology (INCET 2023) during 26th to 28th May 2023.

Dr. Krupa Rasane
Convener - INCET 2023

Dr. J. Shivakumar
General Chair - INCET 2023